Measurement of Strain in Large Structures using the Modal Power Distribution of Embedded Graded Index Optical Fibre Sensors

By
John Maguire B.Sc. (Hons)

A thesis presented
to
Dublin City University

For the degree of Master of Science

September 1995

School of Physical Sciences
Dublin City University
Ireland

Declaration

I hereby certify that this material, which I now submit for assessment on the programme of study leading to the award of M.Sc. is entirely my own work and has not been taken from the work of others, save and to the extent that such work has been cited and acknowledges with the text of my work.

Signed : _John Maguire_   Date : _6/9/95._

TABLE OF CONTENTS

Chapter 5   Data acquisition and Processing

Chapter 6   Results and Conclusions

ABSTRACT

In graded index multimode fibres the transmitted light intensity profile across the face of the fibre is used to monitor the axial strain to which the fibre is exposed. Fibres embedded in concrete, moulded metal and epoxy resin structures were used to detect the strain experienced by the host matrix via the perturbation of the optical power distribution across the cross-section of the fibre core due to stress induced refractive index changes and the resultant exchange of power between optical modes in the waveguide. Intermodal power coupling coefficients were evaluated theoretically for such fibres - in terms of the stress induced refractive index change - and found to be substantial for moderate strains of the order of a few hundred microstrain. The technique cannot differentiate between compressional and extensional axial strains. The system resolution is estimated to be 100 microstrain and the range is unlimited (measurements were made up to a maximum of 2000 microstrain).

Schematic of Stress Induced Mode Power Perturbation In a Parabolic Index Fibre

LIST OF FIGURES

ACKNOWLEDGEMENTS

DEDICATION

To my parents. Thanks for the start.

CHAPTER 1

Introduction to Strain Sensing

The rigidity and useful lifetime of large mechanical structures may be measured by examining the strains within the bodies under load. As buildings increase in size and complexity, it is necessary to be able to continuously monitor the movement of such structures. Similarly, there is a need to examine the forces acting within bridges, dams, and more recently such things as aircraft wings, helicopter rotor blades and pipelines. Ultimately, we want to predict the future occurrence of large deformations and possible failures. The work reported here concentrates on the measurement of internal strains in a selection of host materials by means of embedded optical fibres. Fibre Optic sensors are part of a technology known as Smart Structures and Materials a branch of the science of optical sensing which has emerged over the last ten years. In this chapter, by way of an introduction to the sensing of strain with optical fibres, some key words are defined and fibre optic sensors are introduced. The advantages of fibre embeddment in the sensing of the strain state of large structures over conventional strain gauges are discussed and a mathematical model is developed in which mode coupling in parabolic index fibres due to strain related refractive index changes is discussed.

1.1 Terms and Definitions

Stress : This is the intensity of force, i.e. the force per unit area, acting on a body. It is commonly denoted by the Greek letter σ. If P is the force acting on say a *prismatic bar*[1] of cross sectional area A, then the stress is written

$$\sigma = P/A \qquad\qquad 1.1.1$$

If the bar is compressed then the stress is said to be a Compressive Stress and if it is stretched the stress is a Tensile one. Tensile stresses are defined as positive and compressive stresses as negative. The S.I. units of stress are N/m^2.

Strain : When an axially loaded bar such as that in Fig. 1.1 undergoes a change in length it is said to experience a strain. This strain is said to be positive in the case of a tensile stress acting on the bar and negative for compressive stresses. If L is the original length of the bar and the change in length is δ, then the strain ε is given by

---

[1] A straight structural member having constant cross section throughout its length.

1

$$\varepsilon = \delta \big/ L \qquad\qquad 1.1.2$$

Strain has no units since it is the ratio of two lengths.

Prismatic Bar

L

Bar in Compressive Strain

P→ ←P

δ
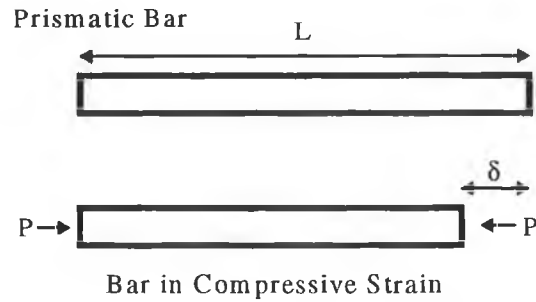
Fig. 1.1 Prismatic bar of length L experiencing
a force P giving rise to a compressive strain ε=δ/L

Stress-Strain Diagrams : A stress-strain diagram is obtained by plotting the strain for different values of compressive or tensile stress. Each material has a characteristic stress-strain diagram. As an example, a stress-strain diagram for a typical steel structure in tension is shown in Fig. 1.2.

Stress

D

B   C   E

A

Strain Hardening

Perfect Plasticity or Yielding

Linear Region
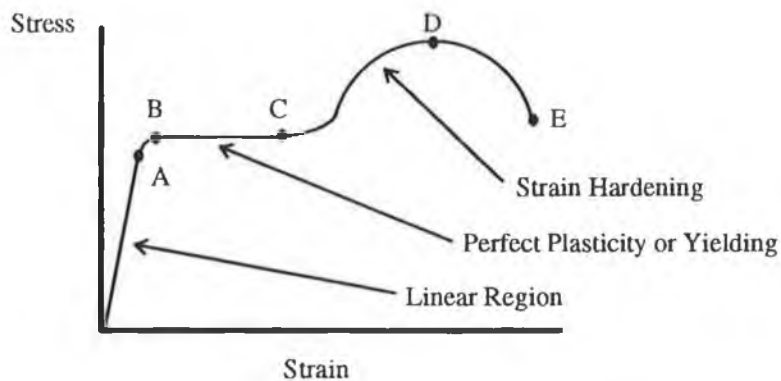
Strain

Fig. 1.2 Typical Stress-Strain Diagram for a steel structure in tension

As can be seen in the diagram, there are several distinct regions in a stress-strain diagram. Starting with the linear region, the stress is directly proportional to the strain. The slope of the

line in the linear region gives the *Modulus of Elasticity*[2]. Beyond the point A, the two are no longer proportional so we say that the stress at A is the proportional limit. As the load is increased beyond the proportional limit the slope decreases until the point B where it becomes zero. The point B is called the yield point after which there is considerable yielding of the material with no noticeable increase in the tensile force. Between B and C the material is said to be perfectly plastic. After the point C the steel starts to *strain harden*[3]. The slope of the graph here is positive until it reaches the point D called the ultimate stress where the slope decreases until finally reaching the fracture point E. The region of interest for the work reported here is the linear region up to the point A.

Elasticity and Plasticity : A material is said to be elastic if it reverts back to its original dimensions when the load under which it has been put is removed. If the material only partially returns to its original shape it is said to be partially elastic. A material undergoes plastic flow when it is loaded in the plastic region. Once the material is loaded within the elastic region it can be loaded and unloaded without affecting the dimensions of the material. However, once the plastic region is entered, the properties of the material change due to changes in the internal structure of the material and the material becomes permanently deformed.

Strain-Gauge : A strain gauge is an instrument which is attached to or embedded within a structure whose strain is to be measured. The three main types are Metal, Semi-conductor and more recently Optical Fibre Strain Gauges. The operation of the Metal and Semi-conductor strain gauges is based on the principle that resistance changes with dimension according to the equation

$$R = \rho \, l / A \qquad\qquad 1.1.3$$

where R is the resistance of the strain gauge, ρ is the resistivity of the material of which it is made and l and A are the length and cross sectional area of the strain gauge respectively. The gauge factor of a strain gauge is given by the equation

---

[2] Defined as the slope of the stress-strain diagram in the linearly elastic region, its value depends upon the particular material being used. Since strain is a dimensionless quantity, the units of the Modulus of Elasticity are the same as that of stress, i.e. N/m^2

[3] The material undergoes changes on the atomic and crystalline level which results in the material gaining an increased resistance to further deformation.

$$g = \frac{\Delta R / R}{\Delta l / l} \qquad\qquad 1.1.4$$

i.e. it is the fractional change in resistance divided by the strain and is a measure of the sensitivity of the transducer. Metal strain gauges are usually made from alloys of Copper-Nickel, Chrome-Nickel or Nickel-Iron and have gauge factors of the order of 2. Semi-conductor strain gauges are composed of small pieces of n- and p-type semiconductor where the p-type resistance increases with increasing strain and the resistance of the n-type decreases with increasing strain. These have a high gauge factor (of the order of 100) and are therefore more sensitive to small changes in strain. These are however much more sensitive to changes in ambient temperature.

One of the main disadvantages of these strain gauges is that they must be bonded to the surface of the structure of interest and therefore cannot convey information about internal strain within the structure. The embedding of optical fibres within structures allows us to examine the state of strain deep within the walls and supporting columns of them. A further disadvantage of the conventional metal and semi-conductor type strain gauges is that they can only sense changes in strain over an area equal to their size. Optical fibre strain gauges allow Distributed Sensing in that a length of fibre can be embedded within a structure and give information about strain anywhere along the fibre using optical time domain reflectometry[4].

Smart Structures & Materials : This is the name given to a technology which has emerged only over the last ten years in which buildings for example are constructed with optical fibres embedded within them. By examining how the propagation of light through the fibres is affected it is possible to determine the state of strain, vibration, movement, damage etc. of the structure. The 'smart' structures convey information to the outside world about themselves. Several large scale structures exist which have fibres embedded within them. As an example, fibre optic strain gauges have been embedded in some of the support tendons of a two span highway bridge in the city of Calgary in Canada [1] and are presently being used to measure the strain in the structure. Similar projects are being carried out at the Winooski One Dam in Winooski, Vermont [2], a railway overpass bridge in Middlebury, Vermont and fibres have been installed, although no work has been carried out yet, in the newly constructed physics building on the campus of Dublin City University. Fuhr, Huston and Ambrose [3] have

---

[4] An Optical Time Domain Reflectometer (O.T.D.R.) is an instrument which measures the back scattered light from an optical fibre due to Rayleigh scattering as well as back reflected light from splices, connectors, faults and the end face of the fibre. The ability to measure the attenuation on an optical link along its entire length makes this technique ideal for distributed sensing.

examined the possibility of the remote monitoring of these installations via the INTERNET global computer network.

Smart materials can be embedded with actuators which allow the structure to shape changes. These so called adaptive structures react against mechanical and chemical changes within the structure itself as well as external environmental influences. A practical example is in aircraft wings where large forces are experienced and vibration suppression, shape control and damage detection are all imperative if safety is to be maintained.

1.2 Fibre Optic Strain Sensors

In fibre optic strain sensing a length of optical fibre is embedded within a host material whose strain state is to be measured. Light propagates through the fibre and some property of this light, for example, polarisation, phase, intensity, wavelength or modal distribution, is used as a measurand from which the strain experienced by the host material can be inferred. It is important that the glass of the fibre makes good mechanical contact with the material within which it is embedded so that the load on the host structure is transferred fully and accurately to the fibre.

Optical fibre sensors have some advantages over conventional ones in that they are light in weight, they are immune to radio frequency interference and noise and they may be used in harsh environments where it may not be possible to have electrical sensors, for example in the petrochemical industry.

The work reported here describes the encapsulation of graded index optical fibres in a selection of host materials and the application of longitudinal compressions and extensions to those composite structures. The transmitted light intensity profile across the face of the fibre was used to detect the strain experienced by the host matrix by examining the perturbation of the optical power distribution across the face of the fibre core. Optical fibre strain gauges in particular while having these advantages have a number of limitations. For instance, they are limited to detecting relatively small strains due to the elastic limitations of fused silica. Another problem is the interference and possible weakening of the host matrix by the embeddment of fibres. In addition, some complicated and sometimes expensive signal conditioning and processing is required in order to determine the strain experienced by a body.

Interferometric sensors are by far the most common type of fibre optic strain sensor. A length of single mode optical fibre acts as one arm of an interferometer. A change in the physical length of the fibre and therefore the path length of a mode within the fibre can be used to infer the strain of the surrounding environment using fringe counting techniques. Single mode fibre optic strain sensing is not without its limitations however and the method of strain sensing described in this text has a number of advantages over interferometric sensing.

- Interferometric sensors require the use of single mode fibre. Graded index optical fibre is easier to produce and thus cheaper than single mode. It is much easier to launch light into a multimode fibre because of the substantially greater core diameter (over 100 μm core radius for multimode fibre whereas that of single mode fibres are of the order of 10 μm or less). Expensive launching equipment is therefore not necessary when using multimode fibre.

6

- Low power light sources which are easy to drive and are inexpensive can be used because as long as all modes are launched into the fibre, i.e. the fibre is 'filled' and any cladding modes inadvertently launched are removed (by means of mode stripping and described later) then a sufficient light intensity at the detector will result.
- While perhaps not as sensitive to very small strains as interferometric sensors are, multimode strain sensors allow measurement of larger strains (100's of μstrain[5]) such as those experienced by real structures like buildings and bridges.
- Multimode fibre optic strain sensors are not as sensitive to vibration in the host material as the interferometric type.

---

[5] μstrain or 1×10^{-6}

1.3 Mathematical Model of Multimode Fibre Optic Strain Sensing using Optical Power Distribution as the Measurand

1.3.1 Modes in Unperturbed Parabolic Index Fibres

By parabolic is meant a cylindrical waveguide in which the refractive index n of the core material - usually Silica glass - changes with distance from the core axis as

$$n^2(r) = n_1^2\{1 - 2\Delta R^2\} \quad R < 1$$
$$n^2(r) = n_2^2 \qquad\qquad R > 1 \qquad\qquad 1.3.1$$

where R is the normalised distance R=r/a and a is the core radius. The parameter Δ is $\left(n_1^2 - n_2^2\right) / 2n_1^2$. The refractive index at the fibre core axis (r=0) is n_1 and n_2 is the fibre cladding material's refractive index which is independent of location in r>a (R>1). The normalised frequency or V number of the fibre is given by

$$V = ka\sqrt{n_1^2 - n_2^2} \qquad\qquad 1.3.2$$

for light of wavenumber k (=$2\pi/\lambda$). The total number of bound modes in such a fibre is approximately

$$N \approx V^2\!/\!4 \qquad\qquad 1.3.3$$

(or about half that for a step index fibre of the same V number).

The modes of the fibre are characterised by discrete values of the propagation constant β and different values of the core mode parameter U and the cladding mode parameter W defined by

$$U = a\sqrt{n_1^2 k^2 - \beta^2}$$
$$W = a\sqrt{\beta^2 - n_2^2 k^2} \qquad\qquad 1.3.4$$

which are related by

$$V^2 = U^2 + W^2 \qquad\qquad 1.3.5$$

In step index multimode fibres the solutions of the wave equation in cylindrical polar co-ordinates (r,φ,z) yield E fields in the core of the form J_l(UR) Cos$l\varphi$ (even modes, Sin $l\varphi$ for odd modes) and K_l (WR) Cos$l\varphi$ in the cladding. Continuity equations at the interface R=1 (i.e. r=a) generate an eigenvalue equation which yields the discrete values of β and hence U and W for each set of four degenerate modes. The term exp i(ωt - βz) applies to each of these field terms (ω is the angular frequency of the optical radiation).

For the parabolic index fibre the solutions of the wave equation are Whittaker functions in the core and Bessel functions K_l(WR) in the cladding. Normalising the E fields at R=1 gives the field values as follows

$$E = \frac{M_{\kappa,\mu}(VR^2)}{M_{\kappa,\mu}(V)} Cosl\varphi \qquad R < 1$$

$$E = \frac{K_l(WR)}{K_l(W)} Cosl\varphi \qquad R > 1$$

1.3.6

This was shown by Yamada and Iwabe (1974) [4].

The mode parameters l and μ are related to κ and m by

$$\mu = \frac{1}{2} \qquad \kappa = \frac{U^2}{4V}$$

1.3.7

and m is the mode index (m=1,2,3...) which is the mth root of the eigenvalue equation

$$2V\frac{M'_{\kappa,\mu}(V)}{M_{\kappa,\mu}(V)} - 1 = W\frac{K'_l(W)}{K_l(W)}$$

1.3.8

where the prime represents differentiation with respect to the argument of the Whittaker function. As before a term exp $i(\omega t - \beta z)$ multiplies each of the fields (core and cladding).

Series expansion for $M_{\kappa,\mu}(VR)^2$ are available in Abramowitz and Stegun (1964) [5] in terms of the confluent hypergeometric Kummer function.

Solutions of the eigenvalue equation 1.3.8 above can be shown to be

$$U^2 = 2V (1 + 2m - 1)$$

1.3.9

(Snyder and Love 1983, Eqn 36-14) [6]

1.3.2 Optical Power Profile in Parabolic Index Fibres (Unperturbed)

In graded index fibres, such as the ones under discussion here, the modes or their associated quasi plane waves, do not propagate with constant angles but change direction continuously inside the fibre. The fibre has a position dependant numerical aperture $\sqrt{n^2(r) - n_1^2}$. If all modes are excited equally by a source and all are attenuated equally in travelling down the fibre then the power distribution at the fibre end equals that at the input. The latter is proportional to the solid angle filled with radiation, and that in turn is proportional to the square of the numerical aperture, i.e. $P(r) \propto [n^2(r) - n_1^2]$

Using equation 1.3.1 we get for a parabolic index fibre

$$P(r) \propto (1 - R^2)$$

1.3.10

as illustrated in Fig. 1.3.
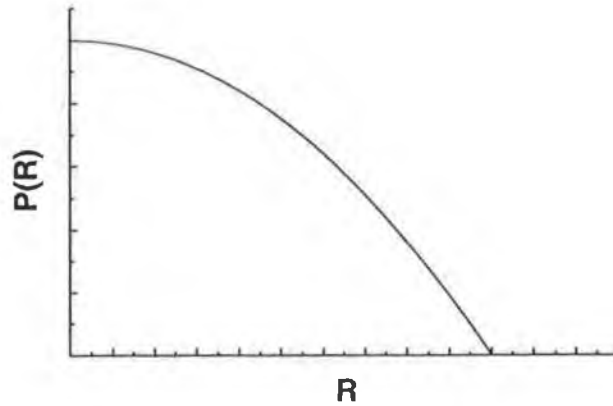
Fig 1.3 Power Profile in a Multimode Parabolic Index Fibre

This is discussed in Gloge and Marcatili (1973) [7]. Thus the power profile of the multimode parabolic index fibre mirrors directly the parabolic refractive index variation in the fibre core. It must be stressed that no perturbations such as bends of small radius of curvature are present in the fibre.

1.3.3 Mode Orthogonality in Unperturbed Fibres

As two mode's E fields $\bar{e}_j$ and $\bar{e}_k$ with propagation constants β_j and β_k both satisfy the same wave equation it can be shown (e.g. Snyder and Love 1983 Section 33.2) that

$$\int_{A_\infty} \bar{e}_j \cdot \bar{e}_k \, dA = 0 \qquad j \neq k \qquad\qquad 1.3.11$$

where the integral is carried out over the cross sectional area of the fibre A_∞. Thus any two (non identical) modes are orthogonal in an unperturbed fibre.

Because of the $Cosl\varphi$ (or $Sinl\varphi$) term in the wavefunctions of Eqn. 1.3.6 the orthogonality equation of 1.3 10 has terms of the form

$$\int_0^{2\pi} Cosl_1\varphi \, Cosl_2\varphi \, d\varphi$$

$$\int_0^{2\pi} Sinl_1\varphi \, Sinl_2\varphi \, d\varphi \qquad\qquad 1.3.12$$

and cross product

$$\int_0^{2\pi} Sinl_1\varphi \, Cosl_2\varphi \, d\varphi \qquad\qquad 1.3.13$$

10

It can be easily shown that

$$\int_0^{2\pi} Cos l_1\varphi \; Cos l_2\varphi \; d\varphi \quad = 0 \; for \; l_1 \neq l_2$$

$$= \pi \; for \; l_1 = l_2$$

$$\int_0^{2\pi} Sin l_1\varphi \; Cos l_2\varphi \; d\varphi \quad = 0 \; for \; all \; l_1 \; and \; l_2$$

$$\int_0^{2\pi} Sin l_1\varphi \; Sin l_2\varphi \; d\varphi \quad = 0 \quad for \; l_1 \neq l_2$$

1.3.14

1.3.4 Stress Induced Refractive Index Changes in Fibres

For many dielectrics the refractive index n and density ρ are related through the Lorenz-Lorentz law

$$\frac{n^2 - 1}{n^2 + 2} = \rho \times \text{constant}$$

1.3.15

When a material is compressed (or extended) the variation in density ρ will give rise to changes in refractive index n (for constant temperature and wavelength). dn/dt for fused silica glass is of the order of 10^{-5} per degree Celsius. The refractive index change Δn with axial strain S_{11} and radial strain S_{12} is given as

$$\Delta n = \left(-n^3 \big/ 2 \right) \left[\left(P_{11} + P_{12} \right) S_{12} + P_{12} \, S_{11} \right]$$

1.3.16

by Davis et al (1986) [8]. For fused silica P_{11}=0.12, P_{12}=0.27 and n=1.46. The radial and axial strain are related by Poisson's ratio ε for the glass which has a value of ε=0.17 for fused silica. Combining constants we get

$$\Delta n = (-0.3170) \left(\Delta L \big/ L \right)$$

1.3.17

for the change in refractive index caused by an axial strain $\Delta L/L$. For compression ($\Delta L/L < 0$) the refractive index increases ($\Delta n > 0$), while for extension ($\Delta L/L > 0$) the refractive index decreases ($\Delta n < 0$).

1.3.5 Mode Coupling Theory

The exchange of optical power between modes in a fibre does not normally occur as the E fields of the various modes are orthogonal. However if the fibre is exposed to a refractive index change, in the core, power can be exchanged between modes. This is treated in Marcuse (1974) [9], Unger (1976) [10] and Snyder and Love (1983) [11] among others.

The basis for the analysis in all cases is the representation of a non uniformity by an induced current density $\bar{J}$ given by

$$\bar{J} = i\sqrt{\frac{\varepsilon_o}{\mu_o}}\, k\left(\bar{n}^2 - n^2\right)\bar{E}$$

1.3.18

(See Snyder and Love Eqn. 22-3)

where $\bar{n}$ represents the refractive index profile in the absence of non uniformities and n is the refractive index in the presence of the non uniformity. The interaction of the $\bar{J}$ vector with the $\bar{E}$ field of a mode gives rise to an energy exchange or coupling of power between modes.

The coupling coefficients between two modes C_{ij} can be written (Snyder and Love Eqn. 28-4)

$$C_{ij} = \frac{k}{4}\sqrt{\frac{\varepsilon_0}{\mu_0}}\frac{1}{(\beta_j - \beta_i)}\int_{A_\infty} e_j^* \cdot e_i \left(\frac{\delta n^2}{\delta Z}\right) dA$$

1.3.19

where * indicates complex conjugation. C_{ij} is related to the contribution da_j to the amplitude of the jth mode due to the excitation by the ith mode by

$$da_j = \frac{ik}{4}\sqrt{\frac{\varepsilon_0}{\mu_0}}\int_{Z_c - \Delta Z}^{Z_c + \Delta Z}(Z - Z_c)\exp i(\beta_i - \beta_j)\, dZ \quad \cdot \int_{A_\infty} e_j^* \cdot e_i \left|\frac{\delta n^2}{\delta Z}\right|_{Z_c} dA$$

1.3.20

(Snyder and Love Eqn. 22-32), the ^ notation indicating unit vectors. In the integrals of 1.3.19 and 1.3.20, the zone of perturbation of the fibre is from

$$Z = Z_c - \Delta Z$$

to $\qquad Z = Z_c + \Delta Z$

The E field normalisations are of the form

$$e_j = \frac{e_j}{\sqrt{N_j}}$$

1.3.21

where

$$N_j = \frac{1}{2}\int_{A_\infty} \bar{e}_j \times \bar{h}_j \cdot z\, dA$$

$$= \frac{1}{2}\sqrt{\frac{\varepsilon_0}{\mu_0}}\int_{A_\infty} n\, e_j^2\, dA$$

1.3.22

and likewise for e_i.

The magnetic field h_j is related to the electric field e_j by

$$\frac{e_j}{h_j} = \sqrt{\frac{\mu_0}{\varepsilon}} = \frac{1}{n}\sqrt{\frac{\mu_0}{\varepsilon_0}}$$

We will now examine how the induced current density J or more particularly the term $\left(\overline{n}^2 - n^2\right)$ is affected by an axial strain in the (parabolic index) fibre. Using Eqn. 1.3.1 we have

$$
\begin{aligned}
\overline{n}^2 - n^2 &= \left(\overline{n}_1^2 - n_1^2\right)\left(1 - 2\Delta R^2\right) \\
&= 2n_1\left(\delta\, n_1\right)\left(1 - 2\Delta R^2\right) \\
&= 2n_1\left(0.3170\, s\right)\left(1 - 2\Delta R^2\right)
\end{aligned}
\qquad 1.3.23
$$

using 1.3.17 to convert a refractive index change to an axial strain s. Inserting 1.3.23 into 1.3.22 we get

$$
\frac{da_j}{dZ} = \frac{-i\, n_1(0.3170)k \int e_i\left(1 - 2\Delta R^2\right)e_j\, R\, dR\, \exp i\left(\beta_j - \beta_i\right)Z}{\sqrt{\int e_j^2\, n\, R\, dR\, \int e_i^2\, n\, R\, dR}}
$$

Now

$$
\int_{-Z_s}^{+Z_s} \exp\!\left(i\left(\beta_j - \beta_i\right)Z\right) dZ = \frac{2 Sin\left(\beta_j - \beta_i\right)^{Z_s}\!\big/_2}{\left(\beta_j - \beta_i\right)}
\qquad 1.3.24
$$

and hence

$$
\left|a_j\right|^2 = -4n_1^2 k^2 (0.3170\, s)^2\, \frac{Sin^2\left(\beta_j - \beta_i\right)^{Z_s}\!\big/_2}{\left(\beta_j - \beta_i\right)^2}\ \times
$$

$$
\left\{ \frac{\int e_i(1 - 2\Delta R^2)\, e_j\, R\, dR}{\sqrt{\int e_j^2(1 - 2\Delta R^2)^{1/2}\, R\, dR\, \int e_i^2(1 - 2\Delta R^2)^{1/2}\, R\, dR}} \right\}^2
\qquad 1.3.25
$$

$|a_j|^2$ represents the power coupled to the jth mode from the ith mode over an interaction region of $z = -Z_s$ to $z = +Z_s$ due to an axial strain s (for light of wavenumber $k=2\pi/\lambda$).

It can be seen from equation 1.3.25 above that the power coupled $|a_j|^2$ scales as s^2 i.e. it is independent of whether the fibre experiences a compressional axial strain $(s<0)$ or an extensional axial strain $(s>0)$.

For a parabolic index waveguide it can be shown (Snyder and Love, 1983) [12]

$$
\begin{aligned}
U^2 &= 2V(l + 2m - 1) \\
a^2\left(n_1^2 k^2 - \beta^2\right) &= 2V(l + 2m - 1)\quad = 2V(M)
\end{aligned}
\qquad 1.3.26
$$

where M is a compound mode index (l+2m-1) for a mode. Differentiating 1.3.26 we get

13

$$-2a^2\beta\,\frac{d\beta}{dM} = 2\,V$$

i.e.

$$\delta\beta = \frac{2\,V\,\delta M}{2a^2\beta}$$

$$\delta\beta \approx \frac{V\,\delta M}{2a^2(n_1 k)} \qquad\qquad 1.3.27$$

Thus equation 1.3.25 reduces to

$$|a_j|^2 = \frac{-16(n_1 k)^4 a^2 (0.3170\,s)^2}{V^2(\delta M)^2}\,Sin^2\left\{\frac{V(\delta M)Z_s}{2(a^2\,n_1\,k)}\right\} \times$$

$$\left\{\frac{\displaystyle\int e_i\,(1-2\Delta R^2)\,e_j\,R\,dR}{\displaystyle\sqrt{\int e_i^{\,2}\,(1-2\Delta R^2)^{1/2}\,R\,dR\int e_j^{\,2}\,(1-2\Delta R^2)^{1/2}\,R\,dR}}\right\}^2 \qquad 1.3.28$$

Because of the $(\delta M)^2$ term in the denominator it can be seen that power coupling will be maximum for $\delta M = 1$ i.e. between modes which are nearest neighbours (l, m) and (l, m+1). Because of the orthogonality conditions of equation 1.3.14 coupling of power will occur between modes of equal l value. l is the azimuthal mode index and is a measure of the number of field maxima on a circumference of the mode pattern. The other index m is the number of field maxima along a radius vector to the mode pattern. It can be seen from equation 1.3.28 that the power coupled between the ith and the jth mode depends on the square of the axial strain of the fibre and is strongest for neighbour modes ($\delta M = 1$). It is predicted then that a fibre exposed to an axial strain will experience a power exchange between modes and as a result, a diffusion of power between modes as illustrated in Fig. 1.4 below.

Strain Zone

Low Power
High Order Modes

Optical Power Diffused
from Low Order Modes
to Higher Ones

High Power
Low Order Modes
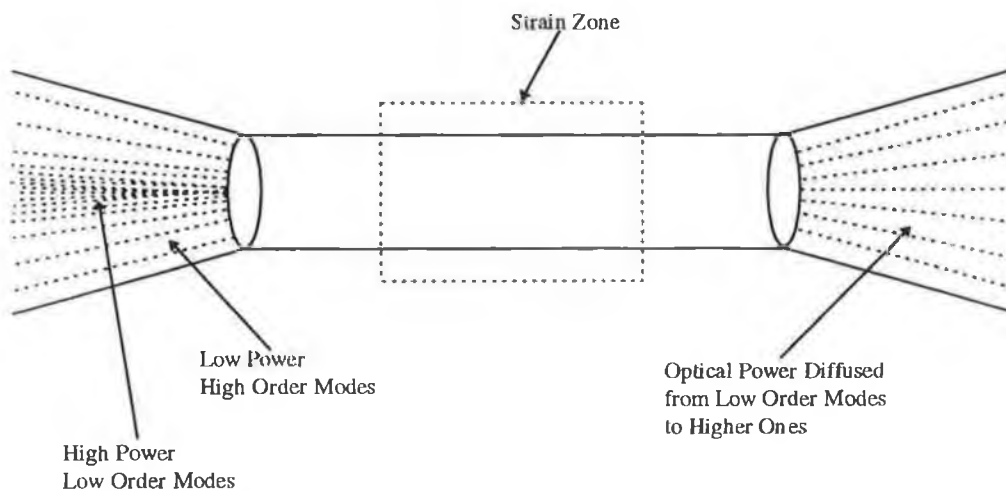
Fig 1.4 Schematic of Stress Induced Mode Power Perturbation
In a Parabolic Index Fibre.

The overall power distribution is thus expected to change from the unperturbed case of Curve A in Fig. 1.5 below to the strained or perturbed case of Curve B.
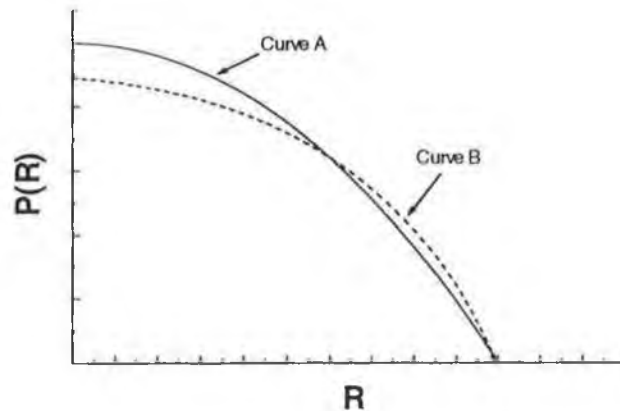
Fig 1.5 Intensity Profiles for Unstrained Fibre (Curve A) and Strained Fibre (Curve B)

1.3.6 Mode Coupling Intensities for Parabolic Index Fibres

A computer program was written to evaluate $|a_j|^2$ from Eqn. 1.3.28 for a parabolic index fibre, the Corning 100/140 CPC3 fibre for which

core radius	$a = 50\mu m$
cladding radius	$b = 70\ \mu m$
acrylate coating radius (nominal)	$125\ \mu m$

It's spectral attenuation decreases from about 4 dB/km at 800nm to about 1 dB/km at 1600nm. It's refractive index profile (as supplied by Corning) is shown in Fig. 1.5
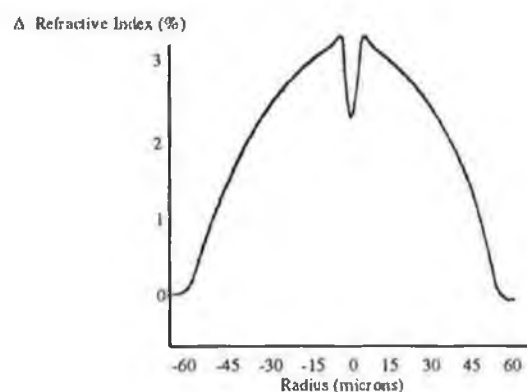
Fig 1.5 Refractive Index Profile for Corning 100/140 CPC3 Optical Fibre

The index profile height parameter Δ - of Eqn. 1.1.1 - is calculated to be 0.0193.

The dip in the refractive index profile near the axis occurs during the manufacturing process using a hollow tube of quartz glass as the preform. At the high temperature necessary to soften the outer glass, some of the dopant (used to create the refractive index profile) diffuses out of the innermost layer and evaporates into the inner tube space before preform collapse occurs. Because of the lower dopant concentration on the axis of the collapsed preform (from which the fibre is subsequently drawn) the refractive index dips to a lower value there.

As a source of light, a Sharp Corp. LT022M50 laser diode of operating wavelength λ = 785nm was used and a strain of 100 microstrain (i.e. 100 x 10^{-6}) was used in the modelling. As the power coupling is predicted to increase as s^2 , power coupling coefficients for any strain value can be easily determined from the single point determination.
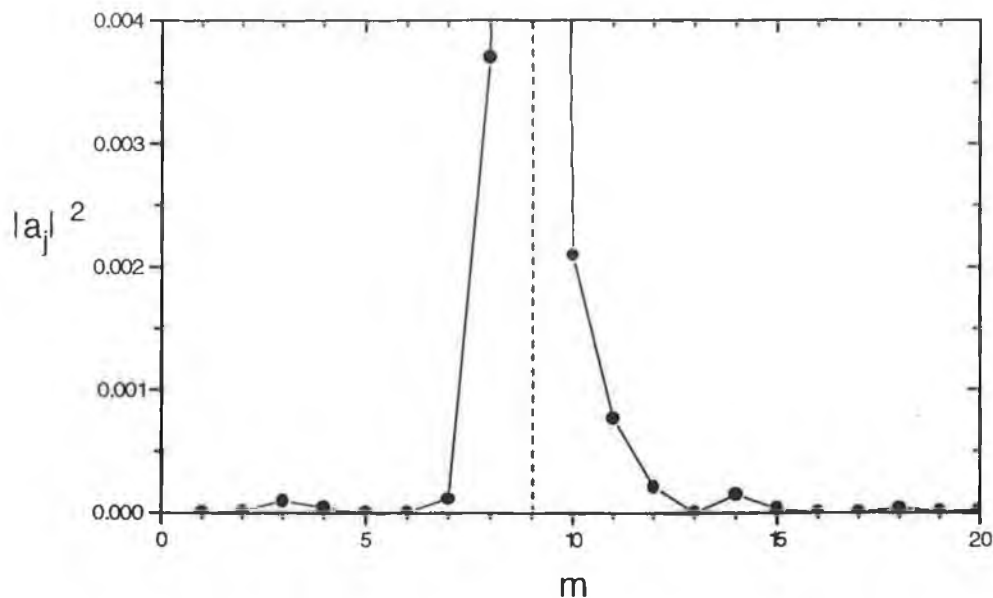
Fig 1.6 Near Neighbour Coupling to the (5,9) mode for 100 µstrain over an Interaction Length of 200 mm.

In Fig. 1.6 above, the power coupling coefficient to the (5,9) mode from the (5,m) modes (m=1...20, m ≠ 9) as determined from Eqn. 1.3.29 using the program listed in Appendix 2 are shown.

As expected, nearest neighbour coupling (from (5,8) and (5,10) modes) is greater than for distant neighbours such as (5,1) and (5,20). At its peak the power coupling coefficient is about 4 x 10^{-3} for a strain of 100 x 10^{-6} and an interaction length Z_s of 200mm.

The same calculation was repeated for a ten fold increase in interaction length, $Z_s = 2m$. This is shown in Fig. 1.7.
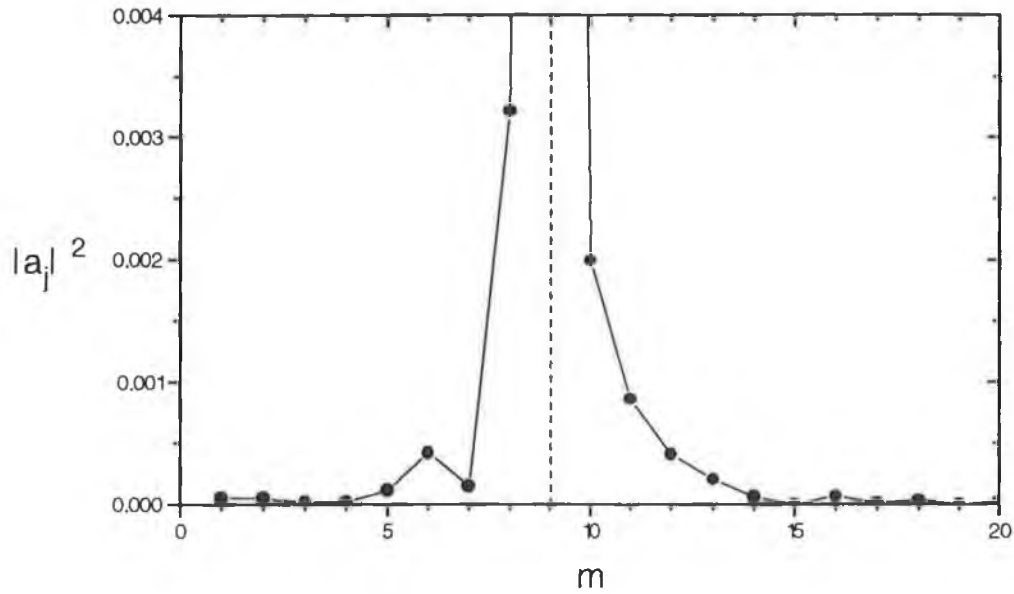
Fig 1.7 Near Neighbour Coupling to the (5,9) mode for 100 μstrain over an Interaction Length of 2m.

It can be seen that the increased interaction length (Z_s from 0.2 to 2m) has not markedly increased power coupling to the (5,9) mode reflecting the Sin^2 ($\Delta\beta\ Z_s /2$) dependence of the coupling coefficient $|a_j|^2$ on Z_s. The Sin^2 term can contribute a maximum of 1.0 to the integral. We examined next how the coupling coefficient $|a_j|^2$ varied for nearest neighbour $\Delta m=1$ coupling, taking as an example the coupling between the (5,m) and the (5,m+1) modes with m varying from 1 to 20. The model predictions are shown in Fig. 1.8. The oscillatory nature of the coupling, reflecting the Sin^2 ($\Delta\beta\ Z_s /2$) term in the coupling coefficient $|a_j|^2$ is seen in the diagram. (strain=100 x 10^{-6} and $Z_s = 0.2m$ as for Fig. 1.7).
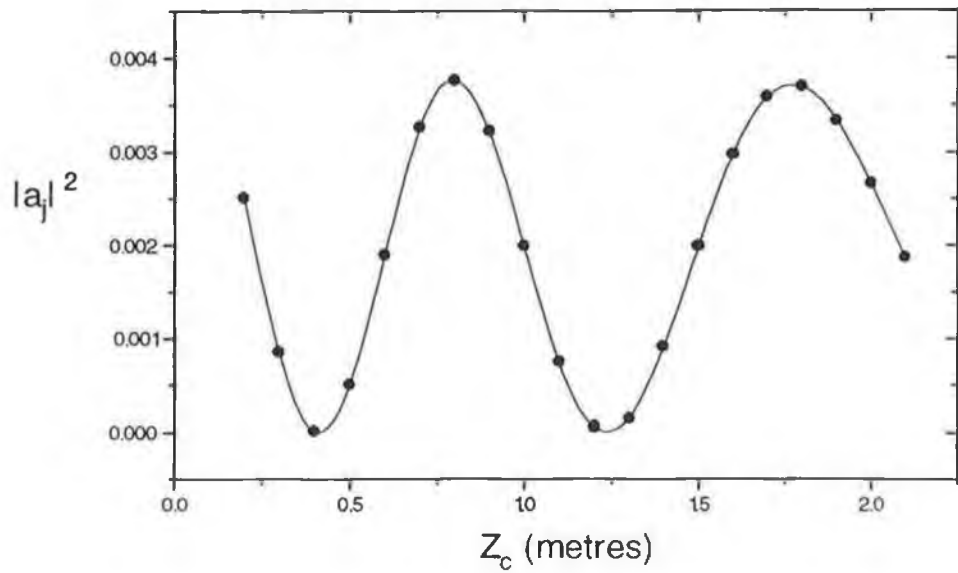
Fig 1.8 Coupling of (5,9) and (5,10) modes as a function of Interaction Length. Strain = 100 x 10^{-6}.
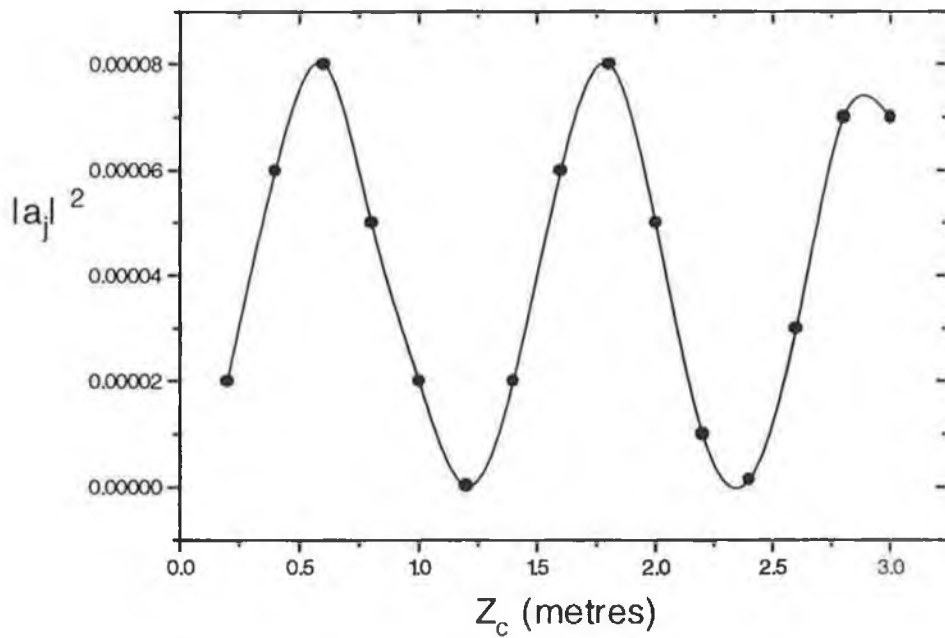
Fig 1.9 Coupling of (5,9) and (5,10) modes as a function of Interaction Length. Strain = 100 x 10^{-6}.
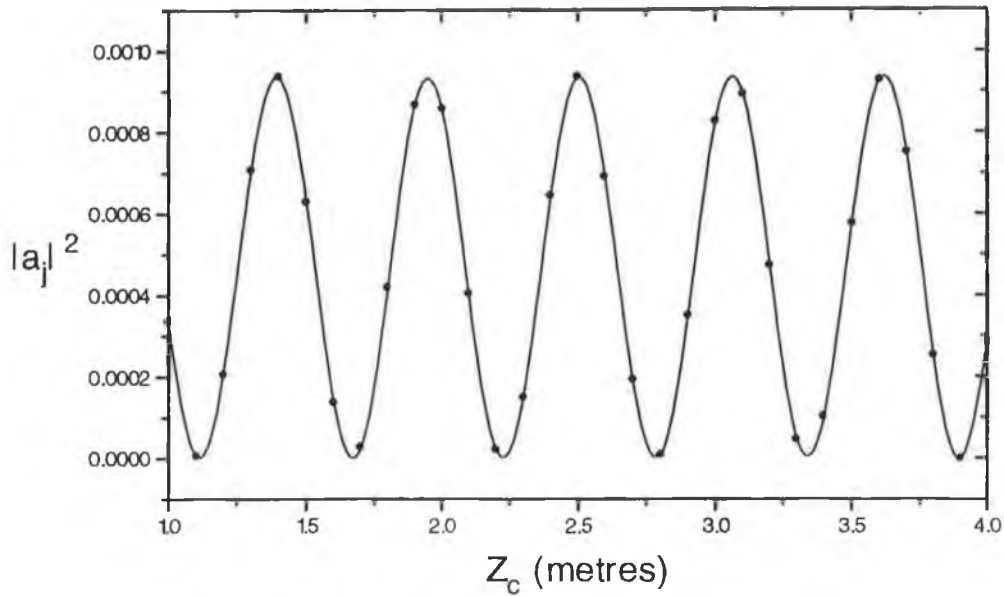
Fig 1.10 Coupling of (5,9) and (5,10) modes as a function
of Interaction Length. Strain = 100×10^{-6}.

All graphs show that coupling coefficients between nearest neighbour modes can be as large
as 0.4% for a strain of 100×10^{-6} (or 40% for 1000×10^{-6} strain) over relatively short lengths
of strained fibre. This predicts that substantial mode coupling or optical power distribution
changes can occur for fibres subjected to strains of a few hundred microstrain over short
interaction lengths (metres or less). Mode coupling in such graded index fibres would, it is
expected, give rise to a diffusion of power from the lower order modes (which cross the axis at
small angles) to higher order ones. It can be seen from Eqn. 1.3.28 that $|a_j|^2$ is zero at certain
values of Z_s corresponding to

$$\frac{V(\delta M)Z_s}{2(n_1 \, ka^2)} = n\pi \qquad n = 0,1,2....$$
<div align="right">1.3.29</div>

This can be seen in Fig. 1.10 above

The net effect of stress induced mode mixing is then predicted to be a substantial coupling of power from the higher intensity low order modes to the lower intensity high order modes or a smoothing of the optical power across all the modes as in Fig. 1.11.
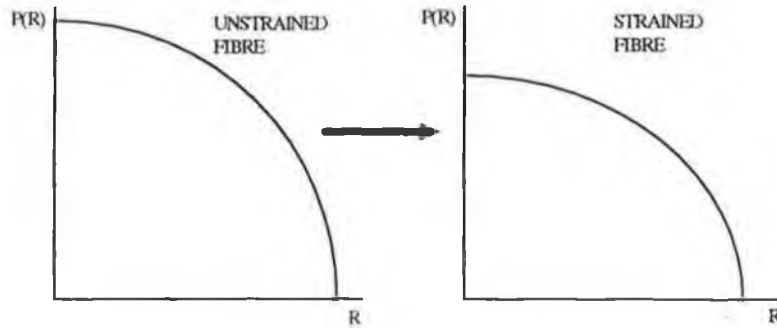
Fig 1.11 Intensity Profiles for Strained and Unstrained Fibres

The detection of this effect in graded index fibres in various matrices to which the axial stress is applied is the purpose of this work.

CHAPTER 2

Review of Previous Work on Fibre Optic Strain Sensing

2.1 Introduction

The use of optical fibres to monitor the strain of an environment in which they are embedded has been the subject of some work. The sensing of strain has been carried out using interferometry in which changes to the physical length of the fibre, and hence the optical path length of a mode within the waveguide, are detected by counting fringes in an interferometer in which the waveguide acts as one arm. In another approach the two polarisation components in a birefringent fibre are allowed to interfere with one another, the degree of interference being strain dependant. A review of these and other methods reported to date in the literature is given below in chronological order. In each case a brief resume of the results reported is given.

2.2 Published Work on Fibre Optic Strain Gauges

Butter and Hocken (1978) [13] used two singlemode fibres as the arms of an interferometer into which laser light was launched using a beam splitter. If the mode propagation constant is β the phase of the light after a propagation distance of L in the waveguide is $\phi = \beta L$. The phase change $\Delta\phi$ can be related to the axial strain ε ($= \Delta L/L$) and given by

$$\Delta\phi = \beta \, \Delta L + L\, \Delta\beta = \beta\, \varepsilon\, L + L\, \frac{d\beta}{dn} + L\, \frac{d\beta}{dD}\, \Delta D \qquad 2.2.1$$

where $\frac{d\beta}{dn}$ is the rate of change of the propagation constant β with core refractive index n; this is approximately equal to β/n. $\frac{d\beta}{dD}$ is the rate of change of the propagation constant with the core diameter D. This can be related to the normalised parameters β and V of the fibre waveguide. The expression for the phase change per unit stress per unit fibre length is then shown to be

$$\frac{\Delta\phi}{\varepsilon L} = \beta - \frac{1}{2}\beta\, n^2 \left[(1-\mu)P_{12} - \mu\, P_{11}\right] + \frac{V^3 \mu}{2\beta D^2}\, \frac{db}{dV} \qquad 2.2.2$$

P_{11} and P_{12} are referred to as the Pockel's Coefficients for the glass of the fibre and are typically $P_{11} \approx P_{12} \approx 0.3$ for silica glass. In a singlemode fibre (V<2.405) $\frac{d\beta}{dV} \approx 0.5$, yielding

$$\frac{\Delta\phi}{\varepsilon L} \approx 1.25 \times 10^7 \, \text{m}^{-1} @ \lambda = 632 \, \text{nm} \qquad 2.2.3$$

The authors cemented two fibres into grooves in a cantilever and found that a displacement of about 10 μm on a 300 mm long cantilever gave rise to a 2π phase change. Their measured sensitivity $\Delta\phi/\varepsilon L$ was 1.20×10^7 m^{-1}. Because of the ambiguity associated with fringe counting i.e. there being no reference level from which to count, the technique is suitable only for small strains less than 1 microstrain in a structure of the order of 1m in length.

Barlow (1989) [14] used a quadrature phase shift detection technique (between the launched optical pulse into a fibre and the transmitted pulse at the far end of the fibre) to detect strain in a multimode fibre cable of gauge length 88m at an operating wavelength of 1300nm. Strains in the range of 0 to 0.07% or 7×10^4 microstrain were detected by this technique.

Mendez, Morse and Mendez (1989) [15] examined the issue of embedding fibre sensors in reinforced concrete structures, the chemical interaction of cement with silica glass, the shrinkage of the concrete on curing and the effect of the aggregates within the concrete on the fibre itself.

McKenzie, Uttanchandani and Soraghaw (1992) [16] investigated the perturbation of the modal pattern in a multimode fibre bonded to a cantilever due to straining of the fibre over a range of 0-200 microstrain. Then using a neural network attempts were made to associate a given speckle pattern with a specific fibre strain.

Spillman, Kline, Maurice and Fuhr (1989) [17] also looked at the changes in the speckle pattern output from a multimode fibre as a function of strain in the fibre. They used a 100/140 μm step index fibre bonded to a metal bar which was fixed at both ends. The bar was driven into transverse oscillation using an electromagnetic vibrator. The speckle pattern was analysed using a 128x128 photodiode array. They concluded that their technique of speckle pattern analysis was suitable to detect vibrations of the structure in which the fibre was embedded.

Herczfeld et al (1990) [18] introduced a multimode step index fibre into a woven 3-D composite consolidated with an epoxy resin and investigated the changes in the modal power distribution (MPD) as the structure was loaded in a direction at right angles to the fibre. By ratioing the optical power at the two angles 0° and 10° stresses in the range 0-100 psi were detected. It was not possible to infer the strain to which the fibre was exposed.

Lee et al (1991) [19] embedded fibre in molten Aluminium and used the cooled structure as an arm of a Fabry-Perot interferometer. Using a 1.3μm distributed feedback laser

source phase shift changes ($\frac{\Delta\phi}{\phi \Delta T}$) of the order of 2×10^{-5} / $^\circ$C were detected. Sensitivity to ultrasonic waves generated in the metal structure was also reported.

Sirkis and Haslach (1990) [20] have investigated theoretically the phase change of light propagating in a single mode fibre which is subjected to an arbitrary strain. Good correlation is reported between the theoretically desired phase change and experimental values obtained for fibres bonded to tip loaded cantilevers. The same authors report (1991) [21] on a range of fibre optic interferometric strain sensors which were surface mounted in a similar fashion to resistance strain gauges. Over a range of 0-250 microstrain, a linear relationship between the experimental and theoretical strain was observed.

Egalon and Rogowski (1992) [22] analysed in numerical models the variation in modal pattern caused by axial strain of a fibre. The analysis applies to few mode fibres i.e. those of low V number.

Habel et al (1994) [23] embedded optical fibres in a concrete matrix to investigate the chemical effect of the silica glass due to the formation of certain chemicals[6] during the hydration reactions in the concrete curing process. Fibres with different coatings were encapsulated for up to 28 days and studied with a scanning electron microscope. Tests concluded that polyimide coatings should not be used for embedding fibres as these coatings were seriously degraded and lost their properties of protection against water and OH ions. A better resistance to attack was demonstrated by acrylate coated fibres.

Habel and Hoffman (1994) [24] achieved a strain resolution of 0.1 microstrain when they embedded extrinsic fibre Fabry-Perot interferometers in a reinforced concrete wall and measured the deformation during the curing of the concrete.

Gusmeroli et al (1994) [25] have simultaneously measured the strain and temperature in a 5m length concrete beam embedded with fibre optic interferometric sensors enabling the thermal expansion of the beam to be measured. These can be measured together as the optical path and dispersion of the fibre are dependant on strain and temperature but with different sensitivities. A thermal expansion coefficient of 11 $\mu\varepsilon$ / $^\circ$ C was reported which agrees with that of reinforced concrete.

Considerable work has more recently been carried out on localised strain sensing using Bragg grating devices. If the refractive index in the core of a fibre is modified - by a chemical change induced periodically along a section of the fibre by holographic techniques using a laser - then a small Bragg grating is impressed into the fibre which will have a high

---

[6] The high alkalinity of fresh cement - the pH can vary from 12.4 to 14.0 - is due to the presence of Calcium Hydroxide and for certain other types of cement, Potassium and Sodium Hydroxide.

optical reflectivity at certain optical wavelengths when the condition $\lambda = 2nd$ is valid. (d is the spacing of rulings in the fibre and n is an integer). By measuring the wavelength of highest reflectivity the grating ruling spacing d can be determined. If d changes due to a strain in the fibre, or the structure in which it is embedded, then the wavelength of highest reflectivity ($\lambda = 2nd$) will also change and the wavelength shift $\Delta\lambda$ will be related to the strain by

$$\varepsilon = \Delta d/d = \Delta\lambda/\lambda \qquad\qquad 2.2.4$$

Because λ is the wavelength of light in the fibre, or its free-space value divided by the refractive index of the core glass (N) the free space wavelength of highest reflectivity will depend linearly on refractive index N. Accordingly any non strain related refractive index changes, such as temperature effects, will introduce ambiguity in the interpretation of λ and $\Delta\lambda$ and effect the strain estimate as well.

Measures et al (1994) [26] used fibre optic intracore Bragg grating sensors to measure the strain relief in steel and carbon composite tendons in a two span highway bridge in the city of Calgary. They carried out their measurements over a period of time and also investigated the effect on the strain due to the dynamic and static loading of the bridge with a truck. With a resolution of a few $\mu\varepsilon$, a strain range of 5000 $\mu\varepsilon$ was achieved. The thermal apparent strain was compensated for by using one Bragg grating within each girder exclusively as a temperature sensor.

CHAPTER 3

Sensor Fabrication

3.1 Introduction

Described below is the design and fabrication process for the three fibre optic strain sensors used during the course of the work reported here. The materials chosen were metal Lead, concrete and epoxy resin. The motivation for choosing them and the relative merits of each material are discussed in their particular sections.

3.2 Metal Lead Sensor

There are a number of reasons for the choice of Lead as the material in which the fibre was to be embedded. The first of these was the fact that Lead has a low melting point relative to the silica glass of the fibre. This meant that it was possible to melt the Lead and pour directly onto the fibre which had been first secured in an Aluminium mould. Initially it was feared that the high temperature of the molten Lead would cause the fibre to shatter due to thermal shock. This however was not observed to occur during the pouring process.

Once the Lead cooled it was expected to contract, squeezing the fibre tightly within the cylindrical piece. This enabled the metal to have good mechanical contact with the glass of the fibre so that the load of the cylinder would be transferred fully and accurately to the fibre.

A mould was made by folding a rectangular piece of Aluminium into a cylinder and placing a flat steel plate underneath. Two jubilee clips served as fasteners for the mould. Through a small slit down the side of the Aluminium plate were placed two curved pieces of stainless steel tubing of internal diameter 1mm and 100mm length as illustrated with the broken lines in Fig. 3.1.

The stainless steel tubes allowed the fibre to exit the Lead without experiencing a strain in the bend. This was necessary as the sensor was to be compressed axially and it was not possible to bring the fibre out through the ends of the cylinder. The tubes also served to reinforce the fibre where it exited the mould and to prevent the primary protective coating from melting and exposing the glass of the fibre.
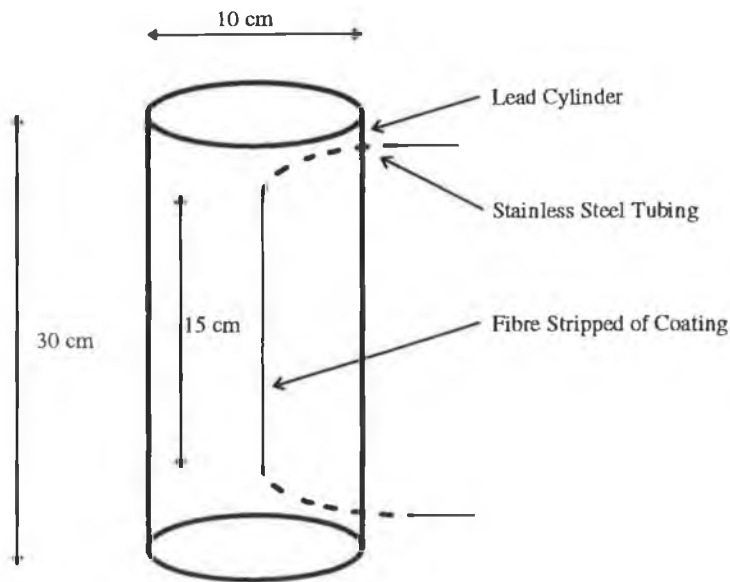
Fig. 3.1 Moulded Lead cylinder with encapsulated fibre

A 100m length of multimode optical fibre[7] was fed through the stainless steel tubing and held in position. The mould was placed in a large container and surrounded by damp sand. This prevented the metal from cooling too fast and thereby contracting too rapidly. A quantity of Lead was melted in a vessel over a hot plate and poured into the mould. When cool enough to handle, the jubilee clips were opened and the Aluminium sheet was peeled away from the Lead cylinder. It was not necessary to remove the primary protective coating of the fibre as this was melted by the molten metal and removed from the fibre during the moulding process.

The contraction of the Lead around the fibre introduced a residual strain on the fibre prior to any loading of the cylinder. This was observed by a dip in the intensity profile near the centre of the fibre[8]. This can be observed in Fig. 3.2 where the total intensity is plotted as a function of the distance from the centre of the fibre . The graph was generated from an actual image taken with the CCD array. This strain in the fibre was not expected to adversely affect the operation of the sensor once it had been calibrated.

The cylinder measured 30 cm in length and 10 cm in diameter.

---

[7] Corning CPC3 100/140 of Numerical Aperture 0.290

[8] This effect is also attributed to the drawing process of the fibre from the preform at elevated temperatures where the dopant material in the core diffuses out from the centre of the fibre.
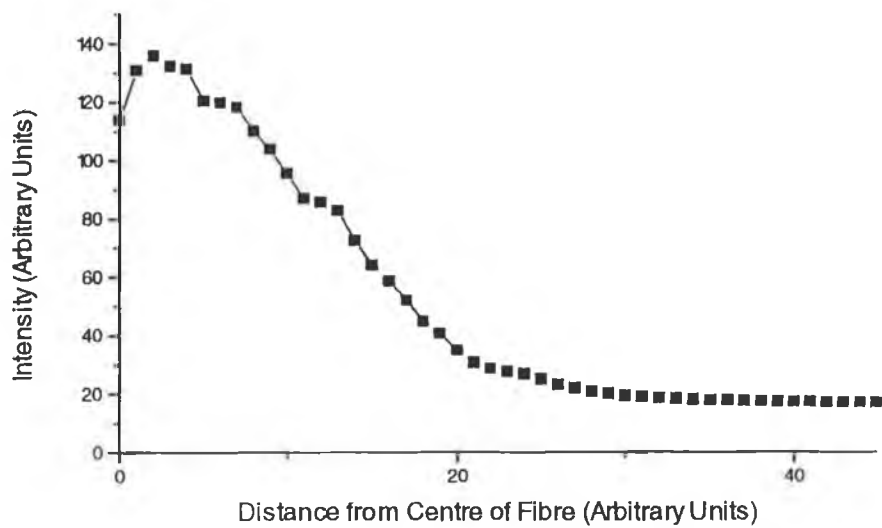
Fig. 3.2 Intensity plotted as a function of distance from the centre of the fibre for the moulded Lead sensor

3.3 Concrete Sensor

Concrete as the composite material in which the fibre was to be embedded was an obvious choice as it is the main construction material in the structures of interest (buildings, bridges, dams etc.). The mix used was three parts to one of fine grain sand and Portland cement. This was combined with approximately 0.7 litres of water. A rectangular Aluminium mould was used. The fibre entered the mould via two stainless steel tubes as described in the previous section. A length of 10cm of the primary protective coating was removed from the fibre with a chemical solvent. This was the sensing length of the fibre.

The fibre was fed through two stainless steel tubes and secured as for the metal Lead sensor. The concrete was then poured into the mould. The sides of the mould were tapped during the course of pouring and afterwards to force any air bubbles in the concrete to the surface. After twenty four hours the concrete block was removed from the mould and placed in a water bath at 21 degrees C for 10 days to *cure*[9]. After the curing process the block was allowed to dry fully. The dimensions of the block were 300x120x100mm as shown in Fig. 3.3.
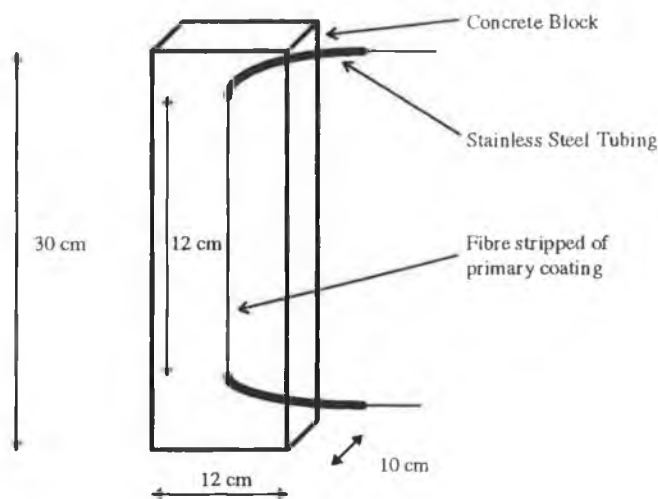
Fig. 3.3 Rectangular concrete block with encapsulated fibre

When tested, it was found that light was unable to propagate through the fibre in the block. The reason for this it is believed was that the lime present in the cement attacked the bare glass of the fibre and caused it to fracture. This meant that the primary coating had to remain on the fibre within the block, possibly leading to an inaccurate and indeterminable transfer of the load on the block to the glass of the fibre.

---

[9] Curing is the process by which the chemical reactions of the ingredients of the concrete mix are accelerated to completion

3.3.1 Modified Concrete Sensor

As for the metal Lead sensor it was important that there was an accurate load transfer from the host material to the glass of the fibre within. Due to the gritty nature of concrete (even with fine grain sand) it was felt that substantial *microbending*[10] power losses would occur with small sand particles pressing against the sides of the fibre. This problem was overcome by first embedding the fibre in metal Lead as before, which was in turn embedded in the concrete block so as to simulate the behaviour of real structures.

A smaller Aluminium mould was therefore made, into which the molten Lead was poured after the fibre had had been secured in the usual manner. When cool the Lead casting with embedded fibre was removed from the mould and placed in the larger mould. The concrete was mixed as before embedding the smaller Lead casting. This arrangement is illustrated in Fig. 3.4. This Lead/concrete combination removed the possibility of microbending in the fibre - due to grit in the sand/cement aggregate - which would lead to optical power loss in the fibre system. It also helped minimise the relative movement of the fibre and the matrix in which it was embedded.

Optical Fibre

Stainless Steel Tubing

Concrete Block

Metal Lead Block with Embedded Fibre
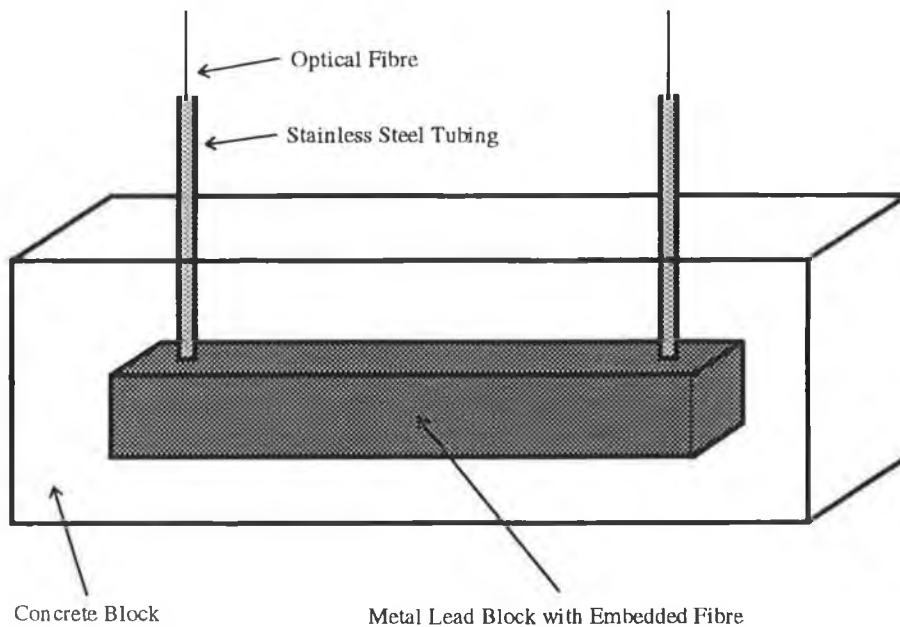
Fig. 3.4 Modified concrete sensor with the fibre encapsulated within Lead which in turn was embedded within concrete

---

[10] The creation of high curvature bends in the fibre due to the pressing of small diameter grit particles into the fibre in this case

3.4 Epoxy Resin Sensor

Optical fibres were embedded in epoxy resin blocks. These had the advantages of easy preparation and pouring, short curing time (8 Hrs.) and no contraction on curing. Two U-shaped Aluminium blocks were bolted onto a flat Aluminium plate, with two rectangular pieces forming the walls of the mould. Gaps were sealed using a Silicone Rubber sealant. A length of 10cm of the fibre's primary protective coating was removed using a chemical solvent and the fibre threaded through two small holes at the end of the Aluminium blocks. These holes were also sealed with Silicone Rubber. The inside walls of the mould were coated with a special *Release Agent*[11] which allows easy removal of the casting from the mould when cured. The resin was prepared by mixing five parts by weight of Epoxide Resin to one part by weight of *Epoxide Hardener*[12]. After pouring into the mould, the mixture was allowed to cure for eight hours at room temperature.

Once cured the side walls of the mould were peeled away and the Aluminium blocks removed from the flat plate. These blocks were then bolted to the platforms of a strain rig. The purpose of the M4 screws was to allow for extension of the piece as well as compression.
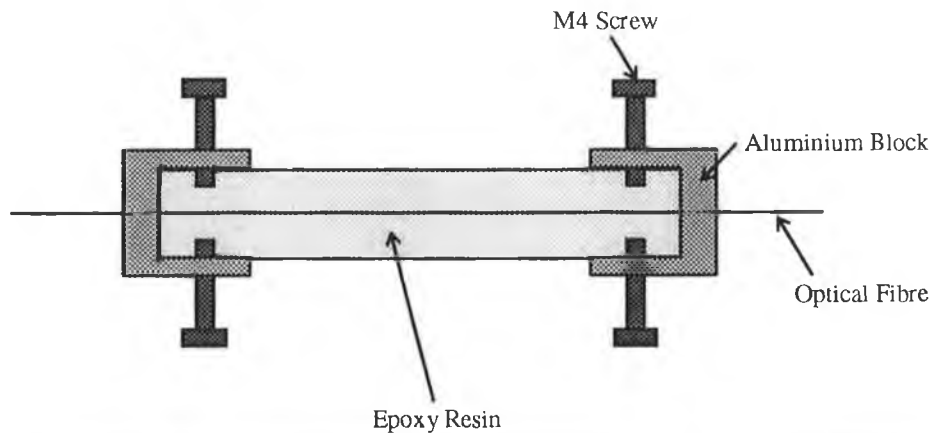
Fig. 3.5 Plan View of Epoxy Resin block with embedded fibre showing the two Aluminium steel blocks and the four M4 screws which allowed the structure to be stretched as well as compressed.

---

[11] BUEHLER Release Agent No. 20-8185-016

[12] BUEHLER Epoxide Resin No. 20-8130-032 and BUEHLER Epoxide Hardener No. 20-8132-008

CHAPTER 4

Optical Configuration of Sensors

4.1 Introduction

This chapter describes the experimental set-up for modal power distribution measurements for each of the three sensors. It details the launch optics used in each case, the light detection equipment, any special work carried out on the fibre or the host material and describes the experimental procedure for obtaining the modal power distribution as a function of the strain experienced by the composite structure. Section 4.5 is concerned with the evaluation of different light sources used and the problems that were encountered when using same.

4.2 Lead Sensor

The experimental set-up for the fibre-in-Lead sensor was as in Fig. 4.1
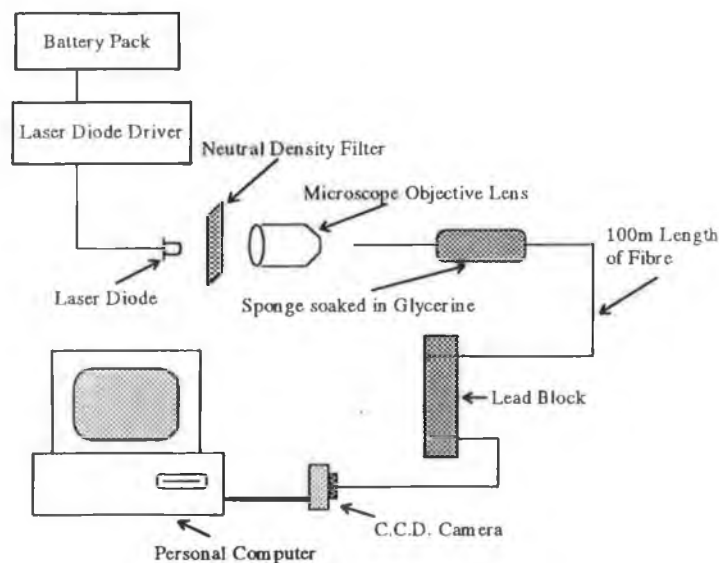
Fig. 4.1 Experimental set-up for metal Lead sensor

Chosen for its high power, the source was an infra-red laser diode[13] with a peak power of 5mW and an operating wavelength of 780nm. It was decided to drive the diode by rechargeable batteries as these would be immune from A.C. mains supply surges. A driver circuit was employed to drive the laser based on a chip supplied with the diode[14] and driven

---

[13] Sharp Laser Diode No. LT022MS0
[14] Sharp Laser Diode Driver Chip No. IR3C02A

from the +/- 4.5 V from the battery pack. A low transmission (1%) neutral density filter served to reduce the intensity and prevent over-exposure of the charged coupled device array. Although not the ideal means of launching light from a laser diode into a fibre (because of the asymmetrical beam), a microscope objective lens was used. This had a numerical aperture of 0.25, close to the N.A. of 0.28 of the fibre. This ensured that nearly all modes of the fibre were being excited. A sponge soaked in glycerine, wrapped around a 10cm length of fibre from which the primary protective coating had been removed extracted light launched into the cladding of the fibre by a process known as mode stripping. A long length of fibre (100m) between source and the Lead cylinder was used to set up an equilibrium mode distribution.

The C.C.D. camera used was the Electrim EDC-1000. The fibre end was cleaved in the usual manner and placed in a brass fibre chuck. This was placed into an XY positioner which was mounted on the camera casing in place of the usual lens arrangement. It was thus possible for the fibre end to be brought close to the C.C.D. array and be positioned over the centre of the detector. The computer displayed in real-time and stored digital images of the light exiting the fibre. Two flat steel plates were placed above and below the Lead block which was put in an Ingstrom Strain Rig. An image was grabbed[15] and saved to disk for different load conditions on the Lead block. These corresponded to different strain values in the fibre. This data was processed by computer software in the manner described in Chapter 5. The experimental results are shown and discussed in Chapter 6.

---

[15] The storage in software of pixel intensities with the C.C.D. camera

4.3 Concrete Sensor

The experimental set-up for compressional loading of the concrete block is shown in Fig. 4.2. The ultra-bright L.E.D. had a peak wavelength of 635 nm and was powered from a +5V power supply with a series resistor to limit the current. The diode current was 30mA. The neutral density filter had a transmission of 1% and served to reduce the intensity of the light launched into the fibre and thus prevent saturation of the C.C.D. The light was focused to a spot of the face of the fibre by means of a microscope objective lens which had a numerical aperture 0.25. This closely matched the N.A. of the fibre (0.28) which meant that light was launched into all possible modes that the fibre could support i.e. the fibre was filled. A sponge soaked in glycerine was wrapped around a 10cm length of fibre from which the primary protective coating had been removed. This was done to remove cladding modes inadvertently launched into the fibre. A large length of fibre was used (80m) so that an equilibrium mode distribution was set up by the time the light reached the concrete block. The concrete block was placed between two flat square steel blocks and then between the jaws of the Ingstrom Strain Rig. The charged coupled device array was the Electrim EDC1000-TE thermo-electrically cooled camera. This was interfaced to a personal computer which enabled acquisition of digital image data for different values of strain of the block.
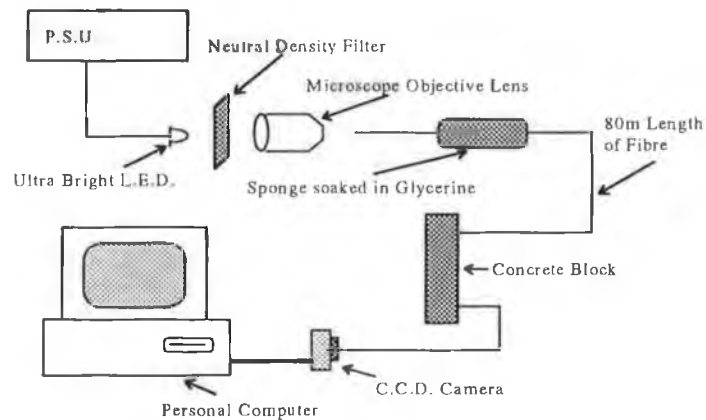
Fig. 4.2 Experimental set-up for concrete sensor

To make the sensor more sensitive to changes in strain, the fibre was passed through the block three times as in Fig. 4.3.
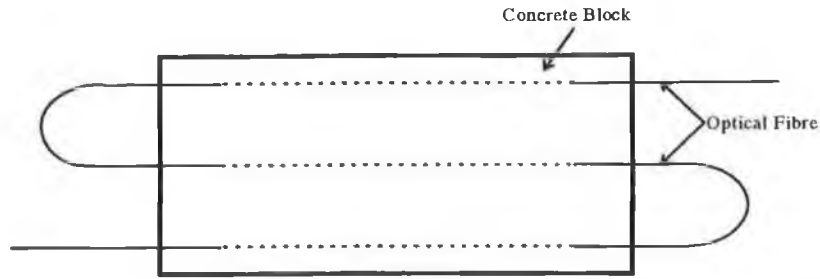
Fig 4.3 Concrete block with multiple passes of fibre to increase sensitivity

With the exposure time of the camera set to 60ms - chosen to avoid over-exposure of the C.C.D. - , the *dark current*[16] was subtracted and an image stored for no load on the block. A load of 1kN was then put on the block and the process repeated. This was done for successive increments of 1kN up to 15kN where the block began to show signs of fracture. - This was the second experiment carried out with this block and it had obviously been weakened. - The data was processed in the manner described in Chapter 5, the results of which are presented in Chapter 6.

---

[16] A feature of all detectors, the Dark Current is the output current even when no light falls on the CCD. In dark current subtraction, an image is saved with no light hitting the CCD and then subtracted pixel by pixel from an unprocessed image to remove unwanted noise.

4.4 Epoxy Resin Sensor

The experimental set-up for the epoxy resin block us shown in Fig. 4.4
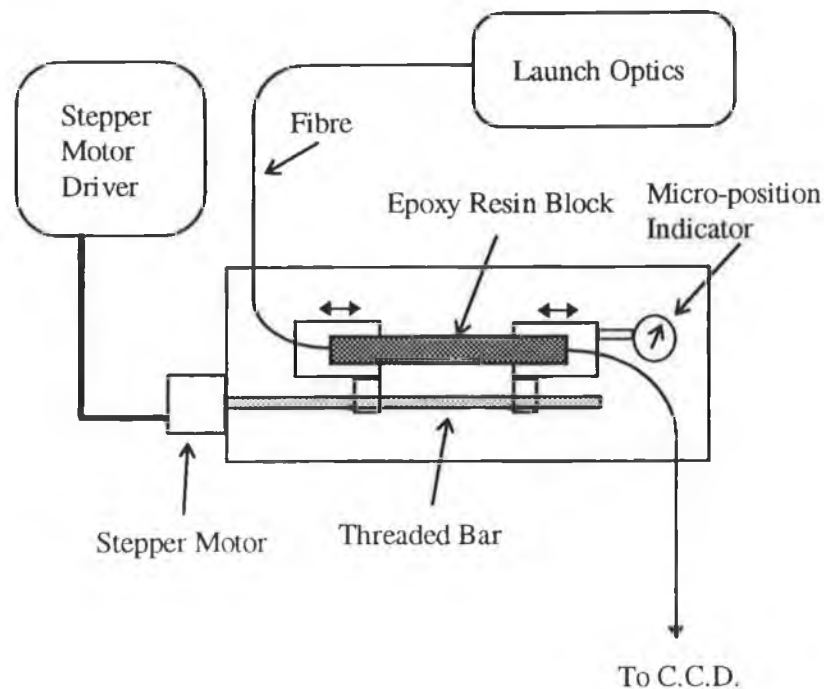
Fig. 4.4 Experimental set-up for epoxy-resin sensor

The launch optics in this case were exactly the same as those used for the concrete block experiments. The end blocks of the epoxy resin sensor were bolted to the two moveable stages which were in turn attached to the threaded bar, turned by the stepper motor of the strain rig. With this particular strain rig it was possible to examine the effect of both compressive and tensile stresses on the fibre. The length of the block was 15cm. It was possible to calculate the strain experienced by the fibre by noting the displacement of the block with the micro-position dial indicator and dividing twice this number (since both ends of the block are displaced) by the original length of the block. Images were taken with the C.C.D. camera as before for different strain values and processed in the usual manner. The results from the work on the epoxy resin block are presented in Chapter 6.

Fluctuations in output radiation (believed due to mode instability of the laser diode with temperature) were observed. In order to clearly see a change in the modal power distribution, some method of referencing the source was required. This was achieved bydividing the value of the power at the centre of the modal intensity pattern as seen by the C.C.D. by a certain value corresponding to the average power of all the pixels in a certain annulus near the edge of the pattern. This method can be used only if we assume that all modes are excited equally by

the source radiation and therefore a fluctuation in the source irradiance will cause the same fractional power change at the centre of the modal power distribution as that near the edge. This referencing also compensated for induced strain effects in the fibre due to ambient temperature fluctuations.

Modal Power Distribution

Annulus Near Edge of
Modal Power Distribution

Intensity(centre)

Normalised Intensity =
Intensity(centre)
Average Intensity of Annulus
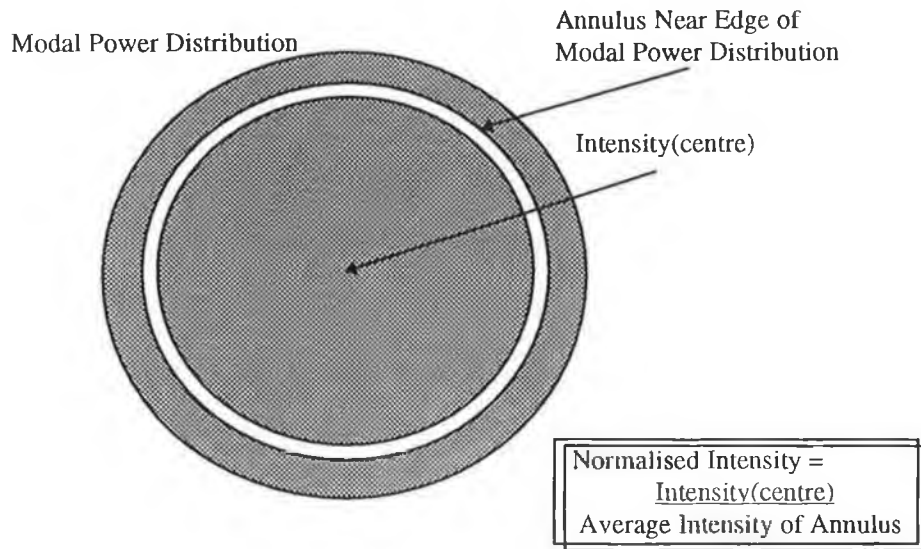
Fig. 4.5 Method of Referencing the Intensity at the centre of the Modal Power Distribution

A second referencing method employed was the one in which two modal intensity patterns were simultaneously imaged on the camera face, one for a fibre under an axial strain, the other for an unstrained fibre. The normalised intensity was obtained by dividing the value of the intensity at the centre of the strained fibre pattern by that of the unstrained fibre.

4.5 Evaluation of Light Sources

As the modal distribution analysis being attempted in this work is an intensity based technique it is critical that light source instabilities be identified and removed if possible. Several light sources were investigated, blue and red LED's and a dark red laser diode. It would appear from Eqn. 1.3.28 that the nearest neighbour mode coupling would be greatest for large values of k i.e. for shorter wavelengths ($k=2\pi/\lambda$). Thus the use of the blue LED (480nm).

The LED's used (red @ 635 nm and blue @480nm) were found to suffer from a progressive reduction in illuminance with time after switch-on. To remedy this, constant current circuits such as that shown in Fig. 4.6 were designed and built. Light power meter measurements indicated a substantial improvement in illuminance stability using such circuits.
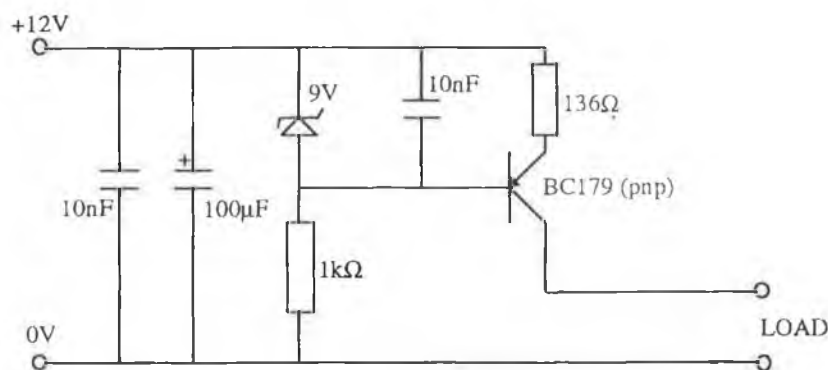
Fig 4.6 Circuit Diagram of LED Constant Current Generator

For the LD used (Sharp Corp. Infrared Laser Diode Number LT022MS0) a current driver circuit based on an integrated circuit supplied by the manufacturers was used. This is shown in Fig. 4.7.
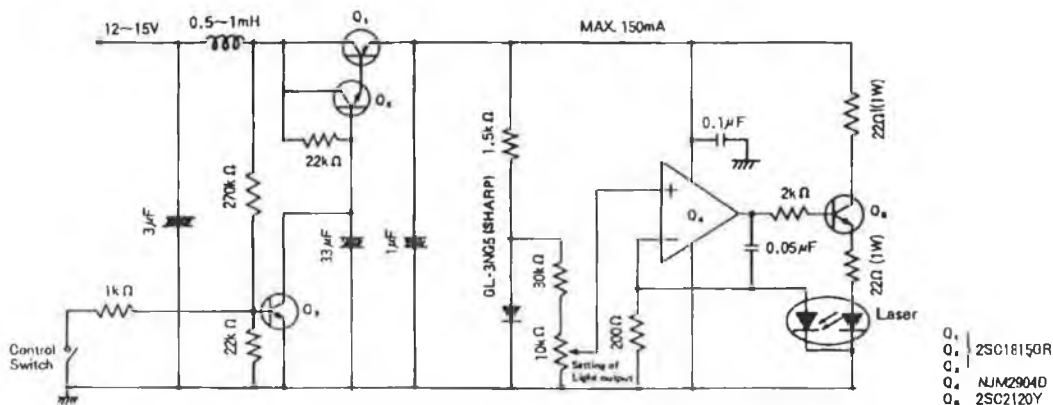
Fig 4.7 Driver Circuit for Sharp LT022MS0 Laser Diode

4.6 Light Launching Optics

The mode filling of the 0.28 numerical aperture Corning parabolic index fibre used was achieved using a microscope objective as shown in Fig. 4.8
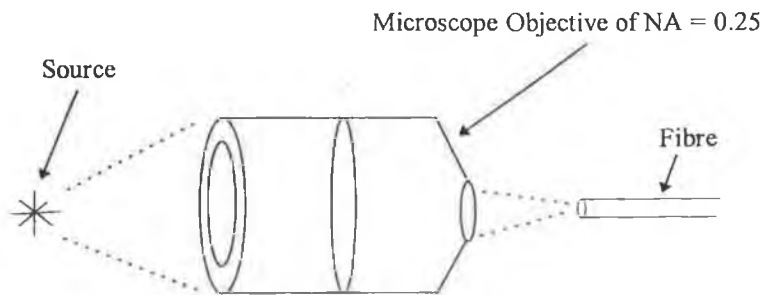
Fig. 4.8 Method of Launching Light into Fibre with Microscope Objective

As the NA of the objective 0.25 was slightly (12%) less than the nominal NA of the fibre (0.28) not all of the fibre modes were excited by the source. The fibre was supported in brass chucks which could be micropositioned in the focal plane of the objective (with three translational axes) using a Newport Fiber Coupler and Newport Fiber Chucks. The LD was held in a drilled Aluminium plate in order to dissipate heat generated by the diode. A photograph of the light launching equipment is shown in Fig. 4.9 which also shows the manner by which the fibre was presented to the C.C.D. camera.
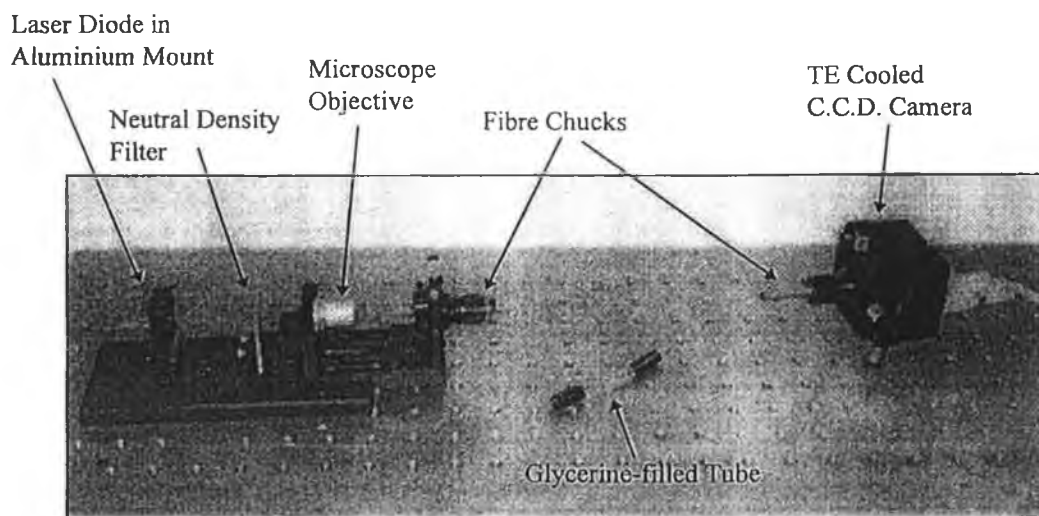
Fig. 4.9 Photograph showing Light Launching and Detection Configuration

38

CHAPTER 5

Data Acquisition and Processing

5.1 Introduction

This chapter describes the process whereby the image data was acquired with the C.C.D. array and processed and the manner in which the value of the intensity at the centre of the modal pattern was extracted from the digital C.C.D. images.

5.2 The Electrim Charged Coupled Device (C.C.D.) and Digital Image Retrieval

The Electrim EDC-1000TE C.C.D. camera was interfaced to a personal computer. The specifications and features of the camera may be found in Appendix 1. Several software packages were supplied by Electrim for the acquisition and processing of digital image data. One such piece of software was called VGACAM.EXE. This was the program responsible for controlling the camera, processing the images and storing the image data to disk.

As described in Chapter 4, the camera software supports dark current subtraction. The dark current is the current produced even with no light falling on the detector. Before the light source was turned on the dark current was saved to the memory of the computer. This was then subtracted pixel[17] by pixel from all subsequent images. The software supplied also allows for the averaging of a number of images to remove unwanted noise. This was achieved by summing together the intensities of any number of images between 0 and 254 and then dividing by the number of images. This averaging together with dark current subtraction was done for each of the images taken with the C.C.D. array.

When storing images with VGACAM.EXE, they are saved in the TIFF format (Tagged Image File Format). This consists of a one dimensional array of 32340 bytes, corresponding to 165 lines of 196 bytes each. The first 4 bytes of each line are not part of the image. The remaining 192 bytes correspond to a row of 192 pixels, each of which is assigned an intensity value of between 0 and 256. A pixel value of zero corresponds to black while white is represented by 256. To be compatible with other software, these have to be converted to the BUF file format. This is achieved using a program called TIF2BUF.EXE supplied with the camera.

A third piece of software supplied with the camera is that called IPS (Image Processing Software). This was used to find the co-ordinates of the centroids of each image i.e. the centre of the image. It was necessary to know the centroids in order to calculate the intensity profile of the image. An explanation of the software responsible for this may be found in the next

---

[17] Abbreviation for picture element

39

section. For a number of images stored in succession, the centroids vary from image to image by only a fraction of a pixel due to small movements in the micro-positioner of the fibre chuck which presents the fibre to the camera active area. Therefore we can assume that the centroids are the same for all images in a particular batch.

5.3 Intensity Profiling Calculation

This software was written in the C programming language. The program called PROFILE.EXE[18] searches the current directory for files with the .BUF extension. On entering the centroids for that particular batch of BUF files the program reads the 192x165 pixel digital image into an array and computes the intensity profiles as follows. An imaginary annulus of a certain thickness h at a radius r is drawn about the centre (found using IPS software) as in Fig. 5.1. Each pixel of the image is examined in turn and if the pixel falls fully within this annulus it's intensity is added to that of all other such pixels. The next annulus of the same thickness is then examined and the intensities summed as before.
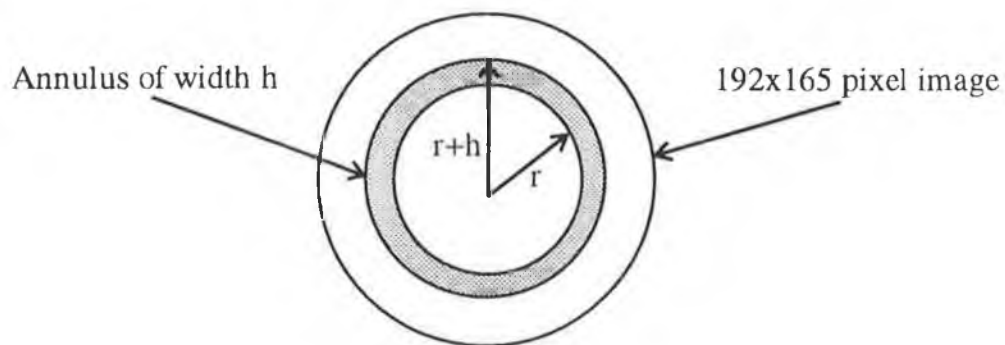
Fig. 5.1 Schematic of Modal Power Distribution exiting fibre with an arbitrary annulus of thickness h

In this manner a total intensity value is obtained for a certain ring of pixels about the centroid and the average intensity for a particular value of distance from the centre of the modal pattern allows an intensity profile to be calculated. A sample intensity profile is shown in Fig. 5.2 where the average power for each annulus is plotted as a function of the distance of that annulus from the centre of the modal intensity pattern.

---

[18] See Appendix 3

41
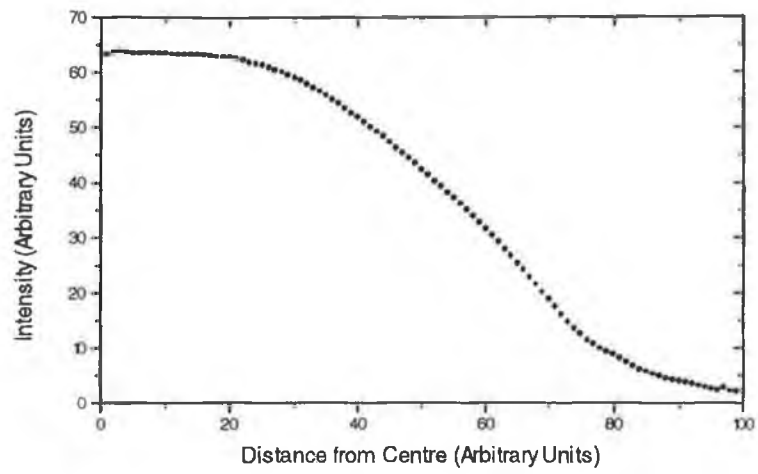
Fig 5.2 Example of an Intensity Profile calculated by PROFILE.EXE

5.3 Intensity Profile Curve Fitting

Each BUF image was processed in the manner described above and a corresponding data file produced containing the intensity information as a function of radius. In Chapter 1 it was predicted that a fibre exposed to an axial strain would experience a power exchange between optical modes from the high power low order modes to the low power high order modes, i.e. the power at the centre of the modal pattern is expected to decrease with increasing strain. To extract the value of the power at the centre of the modal pattern each images data file produced by PROFILE.EXE was plotted and curve-fit to a fourth order polynomial equation of the form

$$y=a-bx+cx^2-dx^3+ex^4$$

Here the **a** coefficient is a measure of the light at the centre of the modal pattern as it is the point at which the intensity profile cuts the y axis.

A program was written in FORTRAN, EPPOLY.EXE[19], which searched the current directory for the data files created by PROFILE.EXE and loaded them individually into the graphing package Easy Plot where they were automatically fit to the polynomial shown above. On fitting the curve the program generated another data file (with the extension .POL) which contained information about the fitting process, the coefficients, the error, the number of iterations etc. A sample POL data file is shown below.

```
"curve generated from eqn:
"   y=a+b*x+c*x*x+d*x*x*x+f*x*x*x*x
"a = +1.6450926208E+002
"b = +6.4284667373E-002
"c = -7.7025689185E-002
"d = +9.5679302467E-004
"f = -3.5943457988E-006

"data points:    99
"iterations:    1167
"sum of errors^2:  1.330027e+002
```

It was thus possible to extract the value of the **a** coefficient. In this manner and by converting the displacement of the block indicated by the dial to a strain (knowing the original length of the block the strain σ = Δl/l), a series of values of **a** coefficients and their corresponding strain was obtained.

---

[19] See Appendix 5

5.4 Summary of Stages Involved in the Extraction of the a Coefficients

- Stage 1 : Save TIFF image

- Stage 2 : Convert to BUF file format (Use TIF2BUF.EXE)

- Stage 3 : Find centre of image (Use IPS software)

- Stage 4 : Calculate intensity profile (Use PROFILE.EXE)

- Stage 5 : Fit polynomial to intensity profile

- Stage 6 : Produce POL data file and extract a Coefficients

- Stage 7 : Normalise a Coefficients by dividing by some Intensity value

- Stage 8 : Plot Normalised a coefficient vs. strain

CHAPTER 6

Results and Conclusions

6.1 Introduction

This chapter described the results obtained with the Epoxy Resin sensors. The strain range of the sensor is discussed as is the noise of the system and the sensitivity of the instrument. These are compared with other reported work. No results were obtained with the metal Lead and Concrete sensors. The reasons why these materials were unproductive are given.

6.2 Metal Lead and Concrete Sensors

When the fibre was encapsulated in Lead (and subsequently in Concrete), the heat treatment of the fibre (at approx. 327°C) while the Lead was molten caused the diffusion of the dopant material in the core of the fibre from the centre and thus a refractive index dip at the centre of the fibre as shown in Fig 6.1.
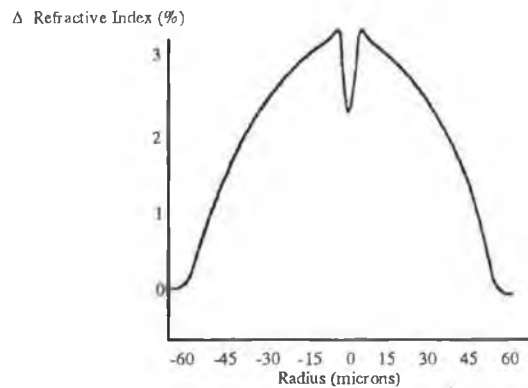
Δ Refractive Index (%)

Fig 6.1 Refractive Index Profile showing dip at the centre of the fibre due to diffusion of dopant from the core at high temperatures

As the power distribution at the fibre end depends on the numerical aperture i.e. $P(r) \propto [n^2(r) - n_1^2]$, there is a corresponding dip in the power at r=0, i.e. the **a** coefficient value. Because of this dip a polynomial fit to P(r) is not good, nor is a measure of the **a** coefficient a good indication of the strain experienced by the fibre. In both the fibre-in-Lead and the fibre-in-Lead and concrete it was observed that with increasing stress the depth of the dip at r=0 decreased. Because of this feature which affects the modelling of the mode coupling process the data presented is restricted to that obtained with the fibre embedded in the Epoxy Resin mould only.

45

6.3 Epoxy Resin Sensor

It can be seen from the data shown in Fig's 6.2, 6.4, 6.5 and 6.6 that the **a** coefficient (which represents the light intensity on the fibre axis which comes from the lowest order modes) decreases with increasing stress (or strain). This parameter can be used as an indication of the strain experienced by the fibre, and if we assume that the load on the structure in which the fibre is embedded is transferred fully and accurately to the fibre, the strain experienced by the matrix in which it is encapsulated.

The **a** coefficient is a measure of the light intensity of the very low order (centre pattern) modes and is, as a result, affected by i) source intensity and ii) C.C.D. camera detection sensitivity. It was decided to normalise the **a** coefficient value using a radial intensity (r>>0) value to make it insensitive to the two factors discussed above.

Fig.'s 6.2, 6.4 and 6.5 show the variation of the 'normalised **a** Coefficient' obtained for the epoxy resin encapsulated fibre under axial stress. Two of the Intensity Profiles (that of the first point and the last point) are shown as Curve 1 and Curve 2 in Fig. 6.3. This clearly shown the decrease in power near the centre of the modal power distribution while the power near the edge (from which the referencing annulus is obtained) remains constant.

The data in Fig. 6.6 is that obtained from the sensor experiencing an axial extension. The data presented here shows that, as predicted in Chapter 1, the mode coupling is independent of whether the fibre experiences an axial compressional strain or an axial extensional strain as the normalised **a** coefficient decreases with increasing strain in both cases. All results were obtained from the Epoxy Resin Sensor constructed from a 5 to 1 mix of epoxide resin to hardener.
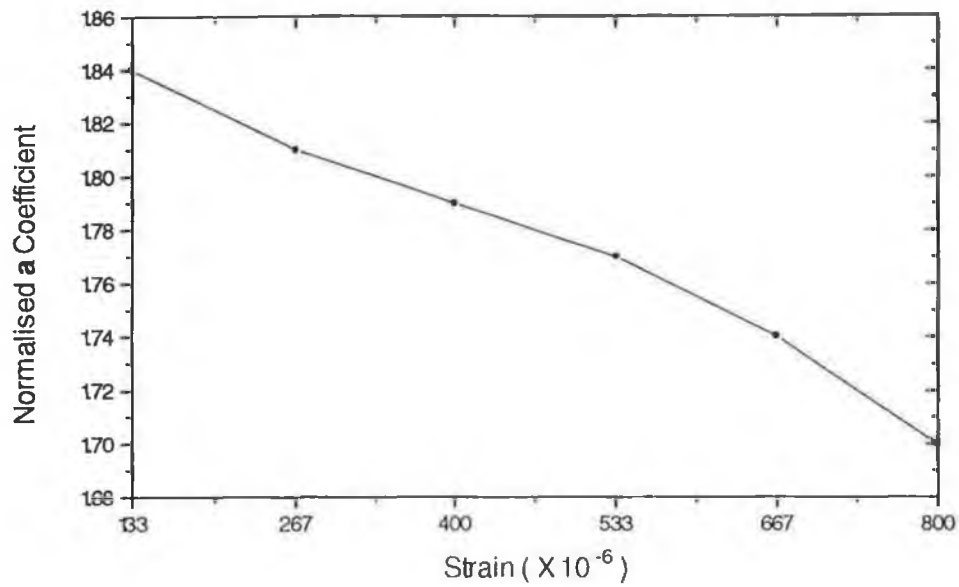
Fig 6.2 Variation of the Normalised a Coefficient with strain for the Epoxy Resin Sensor under Compression
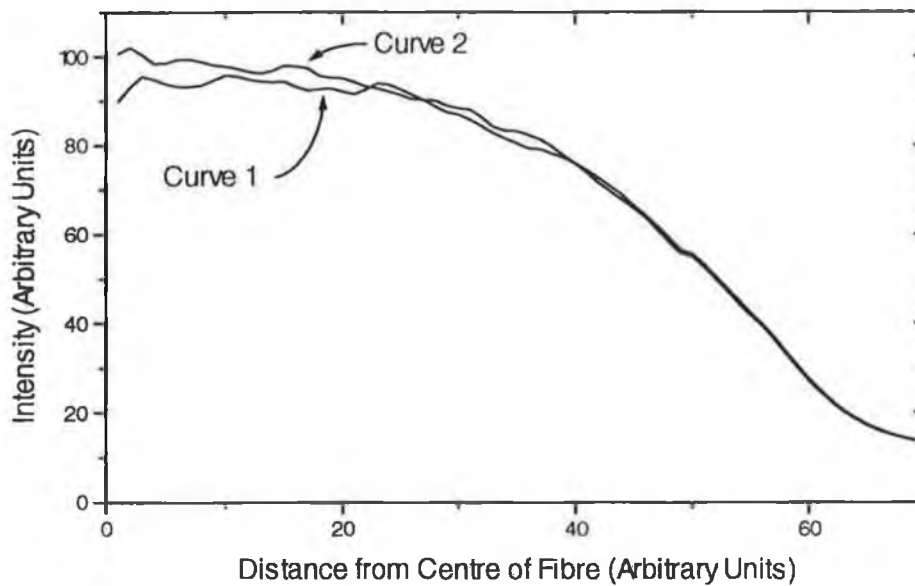
Fig 6.3 Intensity Profiles of two points used to generate the data shown in Fig. 6.2 above, showing central dip due to increased strain on fibre

It can be seen that the a coefficient decreased with increasing strain (either compressional or extensional) reflecting the diffusion of optical power from the lower order modes to the higher order ones as predicted by the theory developed in Chapter 1.

The range of strain measures was from zero to about 2000 microstrain. System noise, which affects the minimum detectable strain change, and is particularly large in Fig. 6.5, is not constant. It was investigated extensively but no reasons for the perturbations of the magnitude shown in Fig 6.5 were found. Using Fig. 6.5 as a 'worst case' measurement the maximum resolvable strain change is about 300 microstrain. At its most stable, the system constructed was able to detect changes of, slightly less than 100 microstrain.
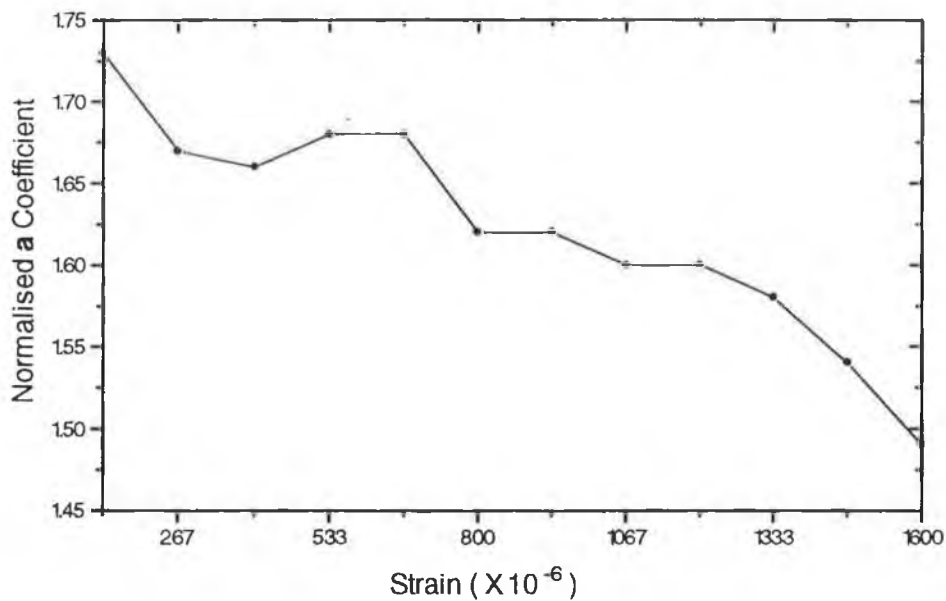
Fig 6.4 Variation of the Normalised **a** Coefficient with strain for the Epoxy Resin Sensor under Compression
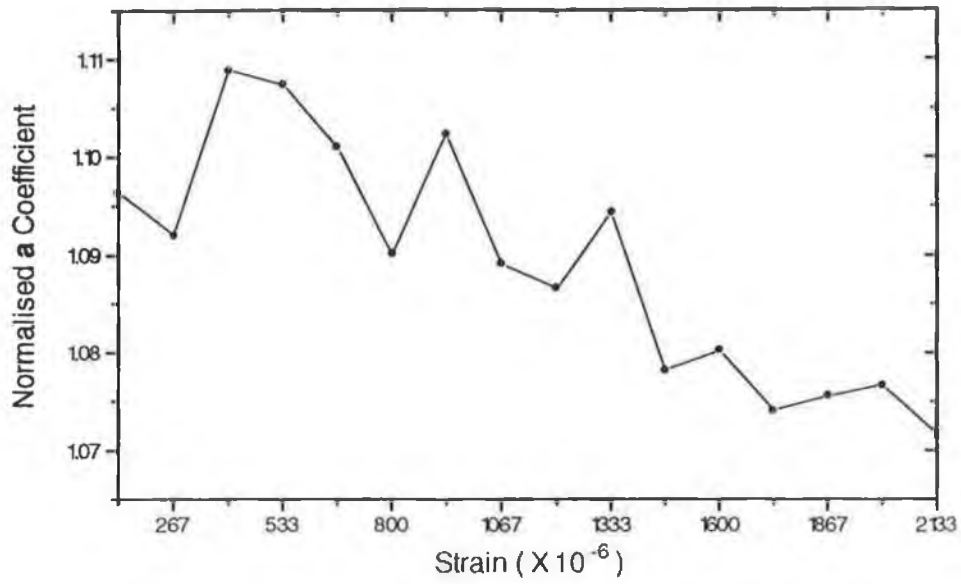
Fig 6.5 Variation of the Normalised a Coefficient with strain for the Epoxy Resin Sensor under Compression
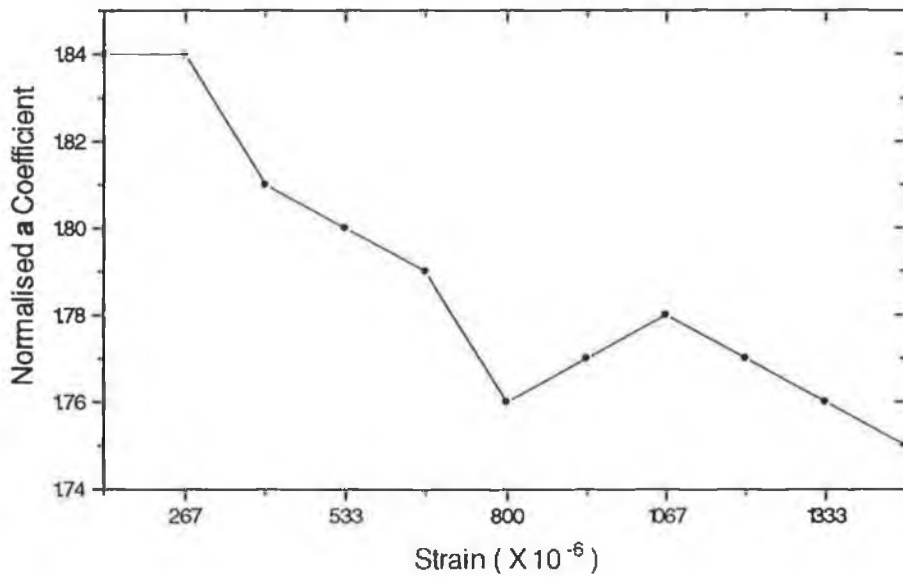
Fig 6.6 Variation of the Normalised a Coefficient with strain for the Epoxy Resin Sensor under Extension

6.4 Conclusions

A fibre optic mode pattern perturbation method to measure the strain of a structure in which the fibre is embedded was demonstrated. Using a laser diode source, parabolic index fibre and a TE cooled C.C.D. camera, the mode pattern modification created by the stress induced changes in the refractive index of the glass of the fibre was measured and related to the strain of the fibre. The technique is suitable for strain measurement in large structures but cannot differentiate between compressional and extensive strains. Like all fibre strain gauge measurements it is sensitive also to changes in ambient temperature but small scale excursions in same (10°C) are not detectable. Further work is required to reduce system noise and thereby increase strain resolution.

REFERENCES

1. Measures TM, Alavie T, Maaskant R, Huang R, LeBlanc M, Bragg Grating Fibre Optic Sensing for Bridges and other Structures, S.P.I.E. Vol 2361, Second European Conference on Smart Structures and Materials, Glasgow (1994)

2. Fuhr PL and Huston DR, Multiplexed Fibre Optic Pressure and Vibration Sensors for Hydroelectric Dam Monitoring, J. Smart Materials and Structures, 2 (1993) 320-325

3. Fuhr PL, Huston DR, Ambrose TP, Remote Monitoring of Instrumented Structures using the INTERNET Information Superhighway, S.P.I.E. Vol 2361, Second European Conference on Smart Structures and Materials, Glasgow (1994)

4. Yamada R and Iwabe (1974), Guided Waves in Optical Square-Law Media, J. Opt. Soc. Am. 64 pp 964-8

5. Abramowitz M and Stegun IA, "Handbook of Mathematical Functions", NBS Washington, Series 55 (1964), Chapter 13, Equations 13.1.32 and 13.1.2

6. Snyder AW and Love JD, "Optical Waveguide Theory", Chapman and Hall, N.Y. (1983)

7. Gloge D and Marcatili EAJ, Multimode Theory of Graded Core Fibres, Bell. Syst. Tech. J. 52 pp 1963-1978 (1973)

8. Davis CM et al, "Fibre Optic Sensor Technology Handbook", (Optical Technologies Inc. 1986), Eqn. 5.3, p5-2

9. Marcuse D, "Theory of Dielectric Waveguides", Academic Press (1974), Chapter 5 - Coupled Power Theory.

10 Unger HG, "Planar Optical Waveguides and Fibres", Clarendon Press Oxford 1976, Chapter 6 - Fibre Imperfections.

11. Snyder AW and Love JD, "Optical Waveguide Theory", Chapman and Hall, N.Y. (1983), Chapter 28 - Local Mode Coupling and Chapter 22 - Non-uniform Fibres

12. Snyder AW and Love JD, "Optical Waveguide Theory", Chapman and Hall, N.Y. (1983), Eqn. 36-14 (Corrected)

13. Butter CD and Hocken GB, Fibre Optic Strain Gauge, Appl. Opt. 17 (18) 2867-2869 (1978)

14. Barlow AJ, Quadrature Phase Shift Technique for Measurement of Strain, Optical Power Transmission and Length in Optical Fibres, J.L.W.T. 7 (8) 1264-1269 (1989)

15. Mendez F, Morse TF and Mendez F, Applications of Embedded Optical Fibre Sensors in Reinforced Concrete Buildings and Structures, S.P.I.E. Vol 1170, Fibre Optic Smart Structures and Skins II 60-67 (1989)

16. McKenzie IA, Uttamchandani D and Soraghan JJ, Applying Image Processing to an Intrinsic Multimode Fibre Optic Strain Sensor, I.E.E. Colloquium on Neural Networks for Image Processing Applications, London (1992) p 6/1-6/4

17. Spillman WB, Kline BR, Maurice LB and Fuhr PL, Statistical Mode Sensor for Fibre Optic Vibration Sensing uses, Appl. Opt. 28 (15) 3166-3176 (1989)

18. Herczfeld PR, El-Sherif MA, Kawase LR and Ko FK, Embedded Fibre Optic Sensor utilising the Modal Power Distribution technique, Opt. Letts. 15 (21) 1242-1244 (1990)

19. Lee CE, Alcoz JJ, Gibler W, Atkins RA and Taytiv HF, Method for Embedding Optical Fibres and Optical Fibre Sensors in Metal Parts and Structures, S.P.I.E. Vol 1588, Fibre Optic Smart Structures and Skins IV (1991)

20. Sirkis JS and Haslach HW Jr., Interferometric Strain Measurement by Arbitrarily Configured Surface Mounted Optical Fibres, J.L.W.T. 8 (10) 1497-1503 (1990)

21. Haslach HW and Sirkis JS, Surface Mounted Optical Fibre Strain Sensor Design, Appl. Opt, 30 (28) 4069-4080 (1991)

22. Egalon CO and Rogowski RS, Model of an Axially Strained Weakly Guiding Optical Fibre Modal Pattern, Opt. Eng. 31 (6) 1332-1339 (1992)

23. Habel WR, Hopcke M, Basedau F and Polster H, The Influence of Concrete and Alkaline Solutions on different Surfaces of Optical Fibres for Sensors, S.P.I.E. Vol 2361, Second European Conference on Smart Structures and Materials, Glasgow (1994)

24. Habel WR and Hofmann D, Strain Measurements in Reinforced Concrete Walls during the Hydration Reaction by means of Embedded Fibre Interferometers, S.P.I.E. Vol 2361, Second European Conference on Smart Structures and Materials, Glasgow (1994)

25. Gusmeroli V, Martinelli M, Barberis A, Escobar P and Morabito P, Thermal Expansion Measurements of a Concrete Structure by Embedded Fibre Optic : An effective example of Simultaneous Strain-Temperature Detection, S.P.I.E. Vol 2361, Second European Conference on Smart Structures and Materials, Glasgow (1994)

26. Measures TM, Alavie T, Maaskant R, Huang S, LeBlanc M, Bragg Grating Fibre Optic Sensing for Bridges and other Structures, S.P.I.E. Vol 2361, Second European Conference on Smart Structures and Materials, Glasgow (1994)

APPENDICES

54

APPENDIX 1

Electrim EDC-1000TE C.C.D. Camera Specifications

Image size / Sensing area	2.64mm x 2.64 mm
Pixel (picture element) size	13.75 x 16 µm
	13.77 x 8 µm (interlaced)
Pixel array (resolution)	192 (H) x 165 (V)
	192 x 330 (interlaced)
Dynamic range and S/N	60dB typical
Non-uniformity	10% typical
Spectral Range	400 - 1100 nm
Peak quantum efficiency	50% @ 700nm
Saturation signal (single scan)	100,000 electrons / pixel
Exposure time	1ms - several minutes
Pixel scan rate	Proportional to computer clock speed
Operating Temperature	32 - 110 ° F

APPENDIX 2

Program : COUPLING.EXE

Language : FORTRAN

Description: This computer program was written to evaluate $|a_j|^2$ from Eqn. 1.3.28 for a parabolic index fibre, the Corning 100/140 CPC3 fibre which has a core radius $a = 50\mu m$, a cladding radius $b = 70\ \mu m$ and an acrylate coating radius (nominal) of $125\ \mu m$. The coupling coefficients for nearest neighbour modes were calculated for a wavelength of 780nm and a strain of $100\ x\ 10^{-6}$. The program was modified to calculate the coupling coefficient as a function of the interaction length Z_c for the same strain value.

$$|a_j|^2 = \frac{-16(n_1 k)^4 a^2 (0.3170 s)^2}{V^2(\Delta M)^2} Sin^2\left\{\frac{V(\Delta M)Z_s}{2(a^2 n_1 k)}\right\} \times$$

$$\left[\frac{\int_\infty e_i(1-2\Delta R^2)e_j\,R\,dR}{\sqrt{\int_\infty e_i^2(1-2\Delta R^2)^{1/2}\,R\,dR\int_\infty e_j^2(1-2\Delta R^2)^{1/2}\,R\,dR}}\right]^2 \qquad 1.3.28$$

```
C       PROGRAM TO CALCULATE WHITTAKER FUNCTIONS
C       VR50.FOR

        IMPLICIT DOUBLE PRECISION (A-H,K,O-Z)
        DIMENSION FAC(0:150),A1(0:1550),B1(0:1550),ANS1(0:1550)
        DIMENSION SUM1(0:1550),ANS4(0:1550),SUM3(0:1550)
        DIMENSION A2(0:1550),B2(0:1550),ANS2(0:1550),ANS3(0:1550)
        DIMENSION SUM2(0:1550),TERM2(0:1550)
        DIMENSION SUM4(0:1550),TERM3(0:1550),TERM4(0:1550)
        DIMENSION TERM1(0:1550),F1(0:1550),E1(1500),E2(1500),XL(5)
        DIMENSION F2(0:1550),XM(5)
C       DEFINE V,L,M,DELTA
C       DEFINE INTERACTION LENGTH(ZC) and STRAIN(ST) in MICROSTRAIN
        ST=100
C       SCAN IN STRAIN LENGTH ZC
        DO 888 NZ=1,40
        ZC=(0.10)*NZ
        DEL=0.0193
        V=(120.0)
        WL=(785.0E-09)
        WN=(6.28319)/WL
        RIZ=1.46
        H=(0.3170)*(1.0E-06)*WN*ST
        CON=WN*RIZ
```

```
      C2=CON*(50.0E-06)
      C3=(C2)**2
      VN=V**(-15.0)
C     DEFINE THE L VALUES OF THE MODES (both the same)
C     DEFINE THE M VALUES OF THE MODES
      DO 500 KJ=5,5
      XL(1)=KJ
      XL(2)=KJ
      DO 501 MJ=10,10
      XM(1)=9
      XM(2)=MJ+1
      IF(XM(2).EQ.XM(1)) GO TO 501
      S1=XL(1)+2*XM(1)
      S2=XL(2)+2*XM(2)
C     DEFINE THE BETA VALUES (prop.constants) FOR THE TWO MODES
      BETA1=CON*(DSQRT(1-2*V*S1/C3))
      BETA2=CON*(DSQRT(1-2*V*S2/C3))
      U1=DSQRT(2*V*(S1-1))
      U2=DSQRT(2*V*(S2-1))
      DELB=BETA1-BETA2
      G=2*H*(DSIN(DELB*ZC/2))/DELB
C     SET UP KAPPA and MU VALUES FOR WHITTAKER FUNCTIONS
C     CREATE THE KUMMER FUNCTION,FROM WHICH WHITTAKER FNS
ARE   DERIVED
      KAPA1=(U1**2)/(4*V)
      KAPA2=(U2**2)/(4*V)
      MU1=(XL(1))/2
      MU2=(XL(2))/2
      C1=0.5+MU1-KAPA1
      C2=0.5+MU2-KAPA2
      D1=1+2*MU1
      D2=1+2*MU2
C     DEFINE FACTORIAL(N),A(N),B(N)
      DO 1 N=1,50
      A1(0)=1.0
      B1(0)=1.0
      A2(0)=1.0
      B2(0)=1.0
      FAC(0)=1.0
      FAC(N)=N*(FAC(N-1))
      CN1=C1+N-2
      IF(CN1.EQ.0) GO TO 50
      A1(N)=(A1(N-1))*(C1+N-1)/(C1+N-2)
      CN2=C2+N-2
      IF(CN2.EQ.0) GO TO 50
      A2(N)=(A2(N-1))*(C2+N-1)/(C2+N-2)
      DN1=D1+N-2
      IF (DN1.EQ.0) GO TO 50
      B1(N)=(B1(N-1))*(D1+N-1)/(D1+N-2)
      DN2=D2+N-2
      IF (DN2.EQ.0) GO TO 50
      B2(N)=(B2(N-1))*(D2+N-1)/(D2+N-2)
      F1(N)=(A1(N))/(((B1(N))*FAC(N)))
      F2(N)=(A2(N))/(((B2(N))*FAC(N)))
```

```fortran
1        CONTINUE
C        CALCULATE WHITTAKER FUNCTION FOR VARIOUS R
         DO 2 J=2,1001
         R=(0.001)*(J-1)
         Z=(R**2)*V
         SUM1(J)=0.0
         SUM2(J)=0.0
         SUM3(J)=0.0
         SUM4(J)=0.0
         DO 3 N=1,50
C        VN IS A TERM PUT IN TO KEEP EACH TERM IN SERIES SMALLISH
         TERM1(N)=(F1(N))*(VN)*(Z**N)
         TERM2(N)=(F1(N))*(VN)*(V**N)
         TERM3(N)=(F2(N))*(VN)*(Z**N)
         TERM4(N)=(F2(N))*(VN)*(V**N)
         SUM1(J)=SUM1(J)+TERM1(N)
         SUM2(J)=SUM2(J)+TERM2(N)
         SUM3(J)=SUM3(J)+TERM3(N)
3        SUM4(J)=SUM4(J)+TERM4(N)
         V2=V/2
         Z2=Z/2
         ANS1(J)=(VN+SUM1(J))*(R**(2*MU1))*(DEXP(V2-Z2))
         ANS2(J)=VN+SUM2(J)
         E1(J)= (ANS1(J))/(ANS2(J))
         ANS3(J)=(VN+SUM3(J))*(R**(2*MU2))*(DEXP(V2-Z2))
         ANS4(J)=VN+SUM4(J)
         E2(J)=(ANS3(J))/(ANS4(J))
2        CONTINUE
10       CONTINUE
4        CONTINUE
         SUMM=0.0
         TSUM1=0.0
         TSUM2=0.0
         DO 30 KK=2,1001
         R=(0.001)*(KK-1)
         TOT1=E1(KK)*E1(KK)*R*(0.001)*(DSQRT(1-2*DEL*R*R))
         TSUM1=TSUM1+TOT1
         TOT2=E2(KK)*E2(KK)*R*(0.001)*(DSQRT(1-2*DEL*R*R))
         TSUM2=TSUM2+TOT2
30       SUMM=SUMM+(0.001)*(DSQRT(1-2*DEL*R*R))*(E1(KK))*(E2(KK))*R*G
         DENOM=DSQRT(TSUM1*TSUM2)
         FS=(SUMM/DENOM)
         FT=FS**2
         NM2=XM(2)
C        WRITE(*,88) NM2,FT
50       CONTINUE
501      CONTINUE
500      CONTINUE
         WRITE(*,889) ZC,FT
888      CONTINUE
5        FORMAT(3(5X,1D12.6))
7        FORMAT(4(5X,1D12.6))
40       FORMAT(I3,2X,I3,2X,I3,2X,I3,5X,I4,2(3X,1D12.6))
100      FORMAT(3(5X,1D12.6))
```

```
88      FORMAT(I5,10X,1D12.6)
201     FORMAT(2(7X,1D12.6))
45      FORMAT(I3,2X,I3,2X,1D12.6)
46      FORMAT(2X,I3,5X,I3,5X,I3,5X,I3,5X,1D12.6)
147     FORMAT(3(5X,1D12.6))
48      FORMAT(2X,1D12.6,5X,1D12.6,5X,1D12.6)
49      FORMAT(10X,1D12.6,5X,1D12.6)
889     FORMAT(5X,1D12.6,10X,1D12.6)
END
```

APPENDIX 3

Program : PROFILE.EXE

Language : C++

Description: This program takes as its input a digital image file in the BUF file format which is an array of 165 rows of 192 light intensity values. The co-ordinates of the centre of the image or centroids are calculated using the IPS software supplied with the Electrim EDC1000TE C.C.D. Camera. These are inserted into the code in the variables xcoord and ycoord. The program calculates the average intensity for a number of rings about the centroids and writes a data file to disk which contains the intensity profile information for that particular image.

```cpp
#include <stdio.h>
#include <stdlib.h>
#include <math.h>
#include <conio.h>
#include <dos.h>
#include <dir.h>

#define ROWS 165
#define COLUMNS 196

unsigned char store[ROWS][COLUMNS], *start;
char c, file1[15], file2[15], p = 0;
FILE *fptr, *ifp;
float xcoord, ycoord, tot, average[160] = {0}, sum[160] = {0};
float lim1, lim2, A[160] = {0};
int total[160] = {0}, i, j, k;
double e2, e4;

void TurnCursorOn ( void);
void TurnCursorOff ( void);

void main ( void )
{
   char drive[10];
   char dir[50];
   char file[50];
   char ext[10];
   int done = 0;
   int done1 = 0;
   char c;
   int FileNumber = 1;
   struct ffblk ffblk;

   done = findfirst("*.BUF",&ffblk,0);
   if (done)
```

```c
{
  printf("Error: No *.BUF Files Found!");
  exit(1);
}
while (!done)
{
    for (i=0; i<100; i++)
    {
      average[i] = 0;
      sum[i] = 0;
      A[i] = 0;
      total[i] = 0;
    }

    clrscr();
    printf("\nPress Escape To Quit..\n\n\n");
    printf("File Number :   %i\n",FileNumber++);
    printf ("Input file  :   ");
    strcpy(file1,ffblk.ff_name);
    printf("%s\n",file1);

    if ((fptr = fopen(file1,"rb")) == NULL)
    {
            printf ("\nError opening .BUF file !");
            exit (0);
    }

    strcpy(file2,file1);
    fnsplit(file2,drive,dir,file,ext);
    strcpy(ext,".DAT");
    fnmerge(file2,drive,dir,file,ext);

    done1 = 0;
    if (access(file2,0) != 0)
        done1 = 1;

    c = '\0';
    while (!done1)
    {
      printf("Output File Exists: Overwrite (Y/N) ?\n");
      while (!kbhit())
      {
        delay(240);
        sound(900);
        delay(240);
        nosound();
      };
      c = getch();
      if (c == 0)
      {
        c = getch();
        continue;
      }
      c = toupper(c);
```

```c
      if (c == 'Y' || c == 'N')
        done1 = 1;

      else
      {
        sound(900);
        delay(240);
        nosound();
      }

    };

    if (c == 'N')
    {
      done = findnext(&ffblk);
      fcloseall();
      continue;
    }
    printf ("Output file :   ");
    printf ("%s\n", file2);

    if ((ifp = fopen(file2,"w")) == NULL)
    {
            printf ("\nError opening .DAT file !");
            exit (0);
    }

    xcoord = 98;
    ycoord = 80;

    printf ("Centroids  :   %3.0f  %3.0f\n\n\n\n",xcoord, ycoord);
    start = &store[0][0];
    TurnCursorOff();
    for (i=0; i<=ROWS; i++)
    {
            printf ("Reading image into array............%3.0f %% done\r", ((i /
165.0) * 100.0));
            for (j=4; j<=COLUMNS; j++, start++)
            {
                    fread(start, 1, 1, fptr);
            }
    }
    fclose (fptr);
    printf  ("\n");

    for (i=0; i<=ROWS; i++)
    {

      if (kbhit())
      {
        c = getch();
        if (c == 27)
        {
          TurnCursorOn();
```

```c
                exit(0);
            }
        }

        printf ("Calculating intensity profile.......%3.0f %% done\r", ((i / 165.0)
* 100.0));

        for (j=0; j<=COLUMNS; j++, start++)
        {
                e2 = sqrt( (pow ((i-0.5-ycoord), 2)) + (pow ((j-0.5-xcoord), 2)));
                e4 = sqrt( (pow ((i+0.5-ycoord), 2)) + (pow ((j+0.5-xcoord),
2)));

                for (k=0; k<100; k++)
                {
                        lim1 = k-1;
                        lim2 = k;
                        A[k] = 1;
                        //A[k] = pow(k, 2) - pow((k-1),2);
                        if ((e2 > lim1) && (e4 < lim2))
                        {
                                sum[k] = sum[k] + store[i][j];
                                tot = tot + sum[k];
                                total[k] = total[k] + 1;
                        }
                }
        }

        for (k=0; k<100; k++)
        {
                if (total[k] == 0)
                        average[k] = 0;
                else
                        average[k] = sum[k] / (A[k] * total[k]);
        }

        for (k=1; k<100; k++)
                fprintf(ifp, "%f\n", average[k]);
        fclose(ifp);

        done = findnext(&ffblk);
};

TurnCursorOn();
for (k = 0; k < 3; k++)
{
   sound(500);
   delay(240);
   nosound();
   delay(240);
   sound(800);
   delay(240);
   nosound();
   delay(240);
}
```

```
}

void TurnCursorOn ( void )
{
  union REGS regs;

  regs.h.ah = 1;
  regs.h.ch = 11;
  regs.h.cl = 12;

  int86(0x10,&regs,&regs);
}

void TurnCursorOff ( void )
{
  union REGS regs;

  regs.h.ah = 1;
  regs.h.ch = 31;
  regs.h.cl = 0;

  int86(0x10,&regs,&regs);
}
```

APPENDIX 4

Program : EPPOLY.EXE

Language : FORTRAN

Description: This program searches the current directory for a text file named EPPOLY.PAR which contains a list of the data files created with PROFILE.EXE and loads them individually into the commercial software graphing package EASYPLOT. Here the intensity profiles are fit with the polynomial described in Chapter 5. For each data file it reads in, another is produced, with a file extension .POL in which the polynomial coefficients among other information is written.

```
      PROGRAM EPPOLY
C
C Program to run EASYPLOT in batch mode

      CHARACTER*12     fnames(150)
      COMMON /NAMES/ fnames, nfiles

C read in filenames to fit
      call READ_PARM

      do 1000 i = 1,nfiles
        write(5,'(1x,i5,2x,a12)') i,fnames(i)
1000  continue

C Create a batch file for EASYPLOT
      ic = 1
1     call MKBATCH(ic)

C Run Easyplot
      call SYSTEM('ep epbatch')

C Rename output file (EP.FIT) from EASYPLOT so that we do not overwrite
      call RNFILE(ic)

C Loop back
      ic = ic + 1
      if(ic .le. nfiles) goto 1

      END
C
C
C
      subroutine RNFILE(ic)

C Routine to rename the EP.FIT file
```

```fortran
        CHARACTER*12      fnames(150),fitname
        CHARACTER*70      fittxt
        COMMON /NAMES/  fnames, nfiles

C Make new *.FIT filename
        fitname = fnames(ic)
        idot=index(fitname,'.')
        fitname(idot+1:idot+3) = 'POL'

        open(unit = 3,file = 'EP.FIT',status = 'old')
        open(unit = 4,file = fitname, status = 'unknown')

        do 100 i = 1,100
          read(3,'(a70)',end=200) fittxt
          write(4,'(a70)') fittxt
100     continue
200     close(3)
        close(4)
        return
        END
C
C
C
        subroutine READ_PARM

        CHARACTER*12      fnames(150)
        COMMON /NAMES/  fnames, nfiles

        open(unit = 1, file = 'eppoly.par', status = 'old')

        nfiles = 0
        do 100 i = 1,150
          read(1,'(a12)', end = 200) fnames(i)
          nfiles = nfiles + 1
100     continue

200     close(1)

        return
        END
C
C
C
        subroutine MKBATCH(ic)
C Make a batch file for EASYPLOT

        CHARACTER*12      fnames(150)
        CHARACTER funct*36,nps*5,ag*4, nm*4, quit*5
        COMMON /NAMES/  fnames, nfiles

        nps = '/tr 2'
        ag = '/ag '
        nm ='//nm'
        quit = '/fq y'
```

```fortran
c       funct = '/tc  y=a*exp(-(x/b)^2)+c'
        funct = '/tc  y=a+b*x+c*x*x+d*x*x*x+f*x*x*x*x'
c       funct = '/tc  y=a+b*x+c*x*x'

        open(unit = 2, file = 'epbatch',status = 'unknown')

        write(2,*) nm
        write(2,*) nps
        write(2,*) ag//fnames(ic)
        write(2,*) funct
        write(2,*) quit

        close(2)

        return
        end
```

APPENDIX 5

Program : EPAPOL.EXE

Language : C++

Description: This program searches the current directory dor the POL data files created with EPPOLY.EXE containing the coefficient information. After promptnig the user for an output file name, the program interrogates the POL files and extracts the **a** coefficient, writing them to the file specified as a list of numbers.

```c
#include <stdio.h>
#include <stdlib.h>
#include <math.h>
#include <conio.h>
#include <dos.h>
#include <dir.h>

FILE *fptr1, *fptr2;
char AString[100], BString[100];
float A;

int IsIn ( char AString[],char ASubString[] );

void main ( void )
{
   char file1[12], outfile[12];
   int done = 0;
   int FileNumber = 0;
   struct ffblk ffblk;

   clrscr();

   printf("Enter output filename....");
   scanf ("%s", outfile);
   if ((fptr2 = fopen(outfile, "w")) == NULL)
   {
        printf ("Error opening output file");
        exit(0);
   }

   done = findfirst("*.POL",&ffblk,0);
   if (done)
   {
     printf("\n\nError: No *.POL Files Found!");
     exit(1);
   }

   while (!done)
   {
```

```c
        printf ("\nProcessing file ");
        strcpy(file1,ffblk.ff_name);
        printf("%s",file1);

        if ((fptr1 = fopen(file1, "r")) == NULL)
        {
            printf ("Error opening input file");
            exit(0);
        }

        FileNumber += 1;
        while (!feof(fptr1))
        {
            strcpy (AString,"");
            fgets(AString,99,fptr1);
            if (strcmp (AString,"") == NULL && !feof(fptr1))
              break;
            if (IsIn(AString,"\"a = +"))
            {
              strncpy(BString, AString, 17);
              strncpy(BString, "               ", 6);
              A = (atof(BString)*10);
              //if (A < 50)
              //   A = A * 10;
              printf ("   a = %.4f", A);
              fprintf (fptr2, "\n%.4f", A);
              fclose (fptr1);
            }
        };
            done = findnext(&ffblk);
    };
    printf ("\n\nNumber of files = %i", FileNumber);
    fclose (fptr2);

}


//----------------------------------------------------------------------
// Function : IsIn ( char [],char [] );
//
// Returns : 1 If ASubString is contained in AString.
//         0 Otherwise
//
//----------------------------------------------------------------------

int IsIn ( char AString[],char ASubString[] )
{
  if (strstr(AString,ASubString))
    return (1);
  return (0);
}
```

APPENDIX 6

Program : ANNULUS.EXE

Language : C++

Description: This program reads each intensirt profile data file created by PROFILE.EXE and extracts the average intensity value of a certain annulus or ring about the centre of the modal pattern. These intensities are written to a separate data file after the user is prompted for a filename. This information allows the **a** coefficients obtained using EPAPOL.EXE to be normalised.

```cpp
#include <stdio.h>
#include <stdlib.h>
#include <math.h>
#include <conio.h>
#include <dos.h>
#include <dir.h>

FILE *fptr1, *fptr2;
char AString[100], outfile[15];
float Num[60], Sum;
int i;

void main ( void )
{
   char file1[12];
   int done = 0;
   struct ffblk ffblk;

   clrscr();

   printf ("\n\n\nEnter output filename   ");
   scanf ("%s", outfile);
   if ((fptr2 = fopen(outfile,"w")) == NULL)
   {
        printf ("\nError opening output file !");
        exit (0);
   }

   done = findfirst("*.DAT",&ffblk,0);
   if (done)
   {
     printf("\n\nError: No *.DAT Files Found!");
     exit(1);
   }

   printf ("\n\n");
   while (!done)
   {
```

```c
    Sum = 0;
    strcpy(file1,ffblk.ff_name);
    if ((fptr1 = fopen(file1, "r")) == NULL)
    {
        printf ("Error opening input file");
        exit(0);
    }


    printf ("\nProcessing file : %s", file1);
    while (!feof(fptr1))
    {
        for (i=0; i<63; i++)
          Num[i] = atof(fgets(AString,99,fptr1));
        printf ("  Intensity at value 60 is %.9f", Num[60]);
        fprintf (fptr2, "\n%.9f", Num[60]);
        fclose (fptr1);
        break;
    };
    done = findnext(&ffblk);
  };
  fclose (fptr2);
}
```